MANY-BODY INTERACTION EFFECTS IN QUASI-ONE-DIMENSIONAL PHOTO-EXCITED ELECTRON-HOLE SYSTEMS

A THESIS
SUBMITTED TO THE DEPARTMENT OF PHYSICS
AND THE INSTITUTE OF ENGINEERING AND SCIENCE
OF BILKENT UNIVERSITY
IN PARTIAL FULFILLMENT OF THE REQUIREMENTS
FOR THE DEGREE OF
DOCTOR OF PHILOSOPHY

by
Kaan Güven
September 1999

I certify that I have read this thesis and that in my opinion it is fully adequate, in scope and in quality, as a dissertation for the degree of Master of Science.

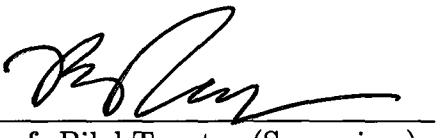

Assoc. Prof. Bilal Tanatar (Supervisor)

I certify that I have read this thesis and that in my opinion it is fully adequate, in scope and in quality, as a dissertation for the degree of Master of Science.

Prof. Atilla Aydınlı

I certify that I have read this thesis and that in my opinion it is fully adequate, in scope and in quality, as a dissertation for the degree of Master of Science.

Prof. Atilla Erçelebi

I certify that I have read this thesis and that in my opinion it is fully adequate, in scope and in quality, as a dissertation for the degree of Master of Science.

U. Salzner

Assoc. Prof. Ulrike Salzner

I certify that I have read this thesis and that in my opinion it is fully adequate, in scope and in quality, as a dissertation for the degree of Master of Science.

Assoc. Prof. Engin Özdaş

Approved for the Institute of Engineering and Science:

Prof. Mehmet Baray,
Director of Institute of Engineering and Science

Abstract

MANY-BODY INTERACTION EFFECTS IN
QUASI-ONE-DIMENSIONAL PHOTO-EXCITED
ELECTRON-HOLE SYSTEMS

Kaan Güven
Doctor of Philosophy in Physics
Supervisor: Assoc. Prof. Bilal Tanatar
September 1999

The work in this thesis concerns many-body interaction effects in a quasi-one-dimensional electron-hole plasma, which may be generated under intense photo-excitation in a semiconductor quantum-well wire. In particular, we investigate how these interactions affect the optical properties of the semiconductor quantum wire. We address this question in two parts: First, the band-gap renormalization (BGR) induced by self-energy corrections of electrons and holes is studied. A two subband model arising from the confinement of the quantum wire is developed to include the multisubband effects. The many-body theoretical formalism of electron (hole) self-energy is given within the GW approximation. We use the dielectric function both in full dynamical random-phase approximation, and in quasi-static approximation, in order to emphasize the dynamical properties of screening. The dependence of BGR on the $e-h$ plasma density, temperature and wire width is studied.

In the second part, the exciton renormalization induced by $e-h$ plasma screening, and Coulomb correlation effects on the optical spectra of a quantum

wire are considered. The optical properties are directly associated with the $e-h$ two particle propogator, which obeys the Bethe-Salpeter equation. Based on recent studies, we review the solution of this equation with screened Coulomb interaction. In particular it is shown* that the dynamical treatment of screening produces an optical absorption/luminescence spectra which is consistent with experimental results. We present a discussion on the interplay of excitons and unbound carriers and on the reflection of this interplay to the optical spectra.

Keywords: Quasi-one-dimensional dimensional electron-hole plasma, self-energy, band-gap renormalization, T-matrix formulation, random-phase approximation.

*S. Das Sarma and D. W. Wang, "Many-body renormalization of semiconductor quantum wire excitons: absorption, gain, binding, unbinding, and Mott transition", cond-matt/9905038

Özet

FOTO-IŞIMA İLE UYARILMIŞ BİREYAKIN BOYUTLU ELEKTRON-DEŞİK SİSTEMLERİNDE ÇOK PARÇACIK ETKİLEŞMELERİ

Kaan Güven
Fizik Doktora Lisansı
Tez Yöneticisi: Doç. Dr. Bilal Tanatar
Eylül 1999

Bu tez çalışması, bireyakın boyutlu elektron-deşik plazmasındaki çok parçacık etkileşmeleri üzerine yapılmıştır. Bu iki bileşenli fermiyon sistemi yoğun foto-uyarılma ile yarı iletken bir kuvantum telinde oluşturulabilir. Tezin konusu olarak, bu etkileşmelerin yarı iletken kuvantum telinin optik özelliklerini nasıl etkilediği üzerinde durulmaktadır. Bu problemi iki bölümde ele aldık: İlk olarak, elektronların ve deşiklerin öz-enerjilerinden kaynaklanan bant aralığı renormalizasyonu incelendi. Sistemin sınırlandırılmasıyla oluşan altbant yapısı iki altbant kullanılarak modellendi ve çoklu altbant etkileri kısmen hesaba katılmış oldu. Elektron (deşik) öz-enerjisinin çok parçacık kuramsal formalizasyonu GW yaklaşımı içerisinde verildi. Dielektrik fonksiyonu hem tam dinamik rasgele-faz yaklaşımı, hem de yarı-statik yaklaşımla ele alınarak perdelemenin dinamik özellikleri vurgulandı. Bant-aralığı renormalizasyonunun $e-h$ plazma yoğunluğu, sıcaklık, kuvantum teli genişliği gibi parametrelere göre nasıl değiştiği araştırıldı.

İkinci bölümde $e-h$ plazma perdelemesi kaynaklı ekziton renormalizasyonunun ve Coulomb korelasyon etkileşmelerinin kuvantum telinin optik

özelliklerine olan etkileri incelendi. Optik özellikler $e - h$ propagatörü ile doğrudan bağlantılıdır, ve bu iki parçacık propagatörü Bethe-Salpeter denklemiyle verilmektedir. Bu denklemin perdelenmiş Coulomb etkileşmesi olduğu durumdaki çözümünü yakın tarihli çalışmalara dayanarak inceledik. Özel olarak, dinamik şekilde ele alınan perdeleme etkilerinin deneysel sonuçlarla uyumlu soğurma/ışıma tayfı oluşturduğu gösterildi.[†] Genel olarak, ekzitonlar ve serbest elektron-deşikler arasındaki etkileşmenin optik tayf üzerine nasıl yansıdığı tartışıldı.

Anahtar sözcükler: bireyakın boyutlu elektron-deşik plazması, öz enerji, bant aralığı renormalizasyonu, rasgele faz yaklaşımı, T-matris formülasyonu.

[†]S. Das Sarma and D. W. Wang, "Many-body renormalization of semiconductor quantum wire excitons: absorption, gain, binding, unbinding, and Mott transition", cond-matt/9905038

Acknowledgement

I would like to express my deep gratitude to my supervisor Prof. Bilal Tanatar, whose personal and academic virtue greatly shaped my approach to scientific study. With his intellectual humour, and friendly attitude, I have enjoyed his guidance throughout my entire Ph.D. study.

I would like to thank Dr. C. R. Bennett, Dr. N. C. Constantinou, and Prof. N. Balkan from the Department of Physics, Essex University, for their hospitality and collaboration during my visit.

I am indebted to my mom, my dad, and my dear sister for their continous support and encouragement. (My particular compliments to my mothers delicious cuisine!)

Here is the crew (though the list is always incomplete!) who helped me to prolongate good times and shorten bad times: Özgür Müstecaplıoğlu (aka Thall) has been a witty companion in our adventures[‡]. Erol Sağol deserves special thanks for his warm friendship and support. Members of our diners club: Hüseyin Boyacı, Okan "Hodja" Tekman, Sencer Taneri. Alpan Bek, Ersin Keçecioğlu, ... Their presence kept me always smiling. Thanks, folks!

I would like to thank to our department secretary Ms. Benderlioğlu, who helped me during the preparation of the manuscript.

And...thank you, Kedi. Simply because, you are there.

[‡]K. Güven and Özgür Müstecaplıoğlu, "Physicist's Quest: An unfinished Tale", (to be published...may be.)

To

Contents

Abstract i

Özet iii

Acknowledgement v

Contents vi

List of Figures viii

1 Introduction 1

2 Subband renormalization effects in a quasi-one dimensional electron-hole system 5

2.1 Confinement Potential and the Effective Coulomb Interaction Matrix 8

2.1.1 The Confinement Potential (Quantum Wire Model) 8

2.1.2 Effective Coulomb Interaction Matrix 9

2.2 The electron(hole) self-energy $\Sigma(k,\omega)$ within the GW approximation 12

2.3 The Dielectric Function 15

2.3.1 The Matrix Polarizability Function $\Pi_{ll'}(q,\omega)$ 17

2.4 Screened Interaction Matrix $\widetilde{W}(q,\omega)$ 19

2.5 Screened Exchange and Coulomb-Hole Decomposition of $\Sigma(k,\omega)$ 21

2.6 The Quasi-static Approximation 23

2.7 LO-phonon interaction effects 24

2.8 Results For The Subband Renormalization 25

2.8.1 Finite Temperature Effects 32
2.9 Coupling to Bulk-LO Phonons 33
2.10 Beyond RPA: The Vertex Corrections 35

3 Many-body effects on optical spectra of semiconductor quantum wires: The interplay of excitons and free carriers 38
3.1 T-Matrix formulation 40
3.2 Low Temperature Limit 44
3.3 Discussion 45

4 General conclusions 48

List of Figures

2.1 The effective Coulomb interaction matrix elements as a function of qR_0. 12

2.2 (a) Dyson's equation for the screened interaction, within the RPA. (b) Electron (hole) self-energy in leading order in the effective dynamical screened Coulomb interaction. 13

2.3 The intra- and inter-subband dielectric functions as a function of q for (a) $\omega = 0$, and (b) $\omega = E_F/2$, respectively. 20

2.4 The intra-subband and inter-subband dielectric functions at $q = k_F/2$ as a function of scaled frequency. 21

2.5 The chemical potential of electrons as a function of density 27

2.6 The chemical potential (dotted line) and the second subband level (solid line) at $N = 1.4 \times 10^6$ cm^{-1} as a function of wire radius. 27

2.7 The subband renormalization as a function of density. 28

2.8 The screened exchange and Coulomb-hole contributions to the subband renormalization as a function of density. 29

2.9 The intra-subband and inter-subband contributions to the subband renormalization as a function of density 30

2.10 The subband renormalization as a function of wire radius at various densities. Solid (dashed) line indicates first (second) subband. 31

2.11 The full dynamical RPA vs. the quasi-static approximation 32

2.12 Temperature dependence of the subband renormalization 33

2.13 Bulk LO-phonon coupling effects 34

2.14 Vertex correction to the basic bubble diagram (shaded bubble). The right hand side represents the expansion in an infinite set of individual vertex lines which couple the propagators (upper and lower branches of the bubble) via the Coulomb interaction. 36
3.1 The Bethe-Salpeter equation for the $e-h$ pair propagator. 40
3.2 Calculated absorption spectra for a GaAs quantum wire structure for various photo-excitation densities by solving the full Bethe-Salpeter equation (a) quasi-static approximation, (b) dynamical approximation. (after Das Sarma *et. al.*[64]) 47

Chapter 1

Introduction

Reduced dimensionality in semiconductor structures reveals intriguing physical phenomena, which drive the interest to study these structures both from a fundamental physics point of view, and from a technological point of view. Two dimensional structures welcomed this interest by resulting in an enormous success in research and device applications. Based on this motivation, it was a natural trend to continue to reduce dimensions of semiconductor structures. Indeed, in the last decade much effort has been devoted to construct true one dimensional and zero dimensional systems, which are commonly referred to as "quantum wires" and "quantum dots", respectively.

It might be instructive to clarify the reduced dimension concept at this point. We are not referring the reduction of dimensions in a strict mathematical sense, but rather as a consequence of the comparison of a length scale associated with physical processes, and the physical size of the system. Thus, reduced dimensionality can arise in many ways, depending on the physical process being considered. For our study, we are mainly concerned with the Fermi wavelength $2\pi/k_F$, as the typical length scale. When a sample dimension becomes comparable to this distance, the motion in that direction becomes quantized, resulting in changes in the energy spectrum and in the dynamical properties of the system. Therefore it is more appropriate to address these systems as "quasi-one-dimensional".

Since the first suggestion by Sakaki[1] and the experimental realization by Petroff *et al.*[2] quasi one dimensional semiconductor structures have been an extensive research area. At present, quantum wires with active widths of about ~ 100 Å, and of negligible thickness have been fabricated.[3,4]

Much of the fundamental theoretical understanding of electrons in one-dimensional systems has come from work on the Tomonaga-Luttinger model.[5,6] The Tomonaga-Luttinger model makes some drastic simplifying assumptions which allow one to solve the interacting problem completely. One surprising result of this model is that any interaction present in the system results in a disappearance of the Fermi surface, leading to a system which is a non-Fermi liquid (in the sense that the elementary excitations are very different from those of the noninteracting system). Therefore, one would expect that experimental properties of semiconductor quantum wires might be very different from any predictions based on the assumption that one-dimensional electron gases are Fermi liquids. However, data extracted from experiments on these structures such as Raman scattering and photoluminescence have proven just the contrary, and shown that the results can be successfully explained on the basis of the standard Fermi-liquid theory. In general, interacting three-dimensional systems with and without disorder, and interacting pure two-dimensional systems are Fermi liquids. It has been shown[7] that in the presence of impurity scattering (which is the case for a real system) one dimensional systems show Fermi liquid behavior, too. Based on these conclusions, we accept the validity of Fermi-liquid behavior without criticizing.

The work in this thesis focuses on some of the nonlinear optical effects in quasi-one-dimensional semiconductor systems, which are induced by many-body correlation effects. It is important to emphasize at the outset that reduced dimensionality by quantum confinement produces not only quantitative but also qualitative differences in the physics of these systems compared to that of bulk structures. The optical absorption spectrum gains some structure associated with quantum-confined electron and hole levels. Excitonic effects become much stronger because of quantum confinement, giving clear absorption resonances

even at room temperature. The relative importance of direct Coulomb screening and exchange effects is different, Coulomb screening being much weaker than in bulk and 2D cases.

The nonlinear optical response is different depending on whether virtual or real $e-h$ populations are generated. In the case of virtual excitations, the amount of time photons spend in an excited state is $\tau \sim \Delta E^{-1}$ where ΔE is the difference between photon energy and excited state energy. Virtual transitions are therefore only favored under off-resonant excitation. The corresponding coherent optical nonlinearities are small, because of the large differences ΔE between photon energies and absorption edge.

Photo-excitation above the absorption edge generates real $e-h$ pairs with no particular quantum-mechanical phase coherence. Due to strong absorption, such resonant excitation produces a large number of electrons and holes for a given laser intensity, and hence significant changes in the optical properties of the material. After being generated, electrons and holes undergo a number of relaxation processes; the changes they induce in the optical spectra are therefore limited to their lifetime. In semiconductors, they can form bound (exciton) or unbound ($e-h$ plasma) states, which produce different effects. There are two relaxation times which should be distinguished. First is the time it takes the photo-excited electron and hole to reach a thermodynamic equilibrium among themselves. This lasts usually a fraction of a picosecond, thus the quasi-equilibrium assumption is well justified unless one deals with ultrafast optical processes. Second, is the time it takes electrons and holes to equilibrate with the lattice (in the picosecond range). Excitons that are generated by resonant excitation within the absorption peak are only stable at low temperatures. Since the two species have different effects on optical spectra, it is necessary to distinguish among them experimentally and theoretically. Our aim is to consider separately degenerate $e-h$ plasma effects and excitonic effects on band-gap and optical absorption. We assume a dense electron-hole plasma generated under intense photo-excitation, thus, emphasis will be on effects due to free carriers. Yet, within the density range of interest, excitons are present on the low-density

part, and should be taken into account. We do this by formulating the problem as a single exciton embedded in a degenerate $e-h$ plasma.

The thesis is organized as follows: In chapter 2, we describe the band-gap renormalization phenomenon in semiconductor structures and consider renormalization in a quantum wire. The subbands formed by the quantum confinement are taken into account. This leads to renormalization of the subband levels, and hence of the fundamental band-gap of the wire material. The dependence of renormalization on $e-h$ plasma density, wire width, temperature will be discussed. Chapter 3 gives a review of recent studies concerning Coulomb correlation effects on optical spectra from quantum-confined systems, with emphasis on quasi-one-dimensional structures. Formation and stability of excitons in the presence of e-h plasma, and their optical properties are discussed. We conclude with general remarks in chapter 4.

Chapter 2

Subband renormalization effects in a quasi-one dimensional electron-hole system

When a dense electron-hole plasma is generated in an intrinsic semiconductor by intense photo-excitation, exchange-correlation effects among the carriers modify the properties of the semiconductor which are based on a single particle approach. In particular, the band-gap of the material is reduced, which is usually referred to as the "band-gap renormalization" (BGR) effect. Renormalization causes increasing absorption in the spectral region below the lowest exciton resonance. As substantial amount of carrier population may be induced by optical excitation, the renormalized band gap can affect the excitation process in turn and lead to optical nonlinearities. Band gap renormalization as well as various optical properties of the Q1D electron-hole systems have been studied[7–11] similar to the bulk (3D) and quantum-well (2D) semiconductors[12–14] where generally good agreement with the corresponding measurements[15–17] exist.

Density dependence of the BGR in Q1D systems was first considered by Benner and Haug[8] within the quasi-static approximation. Hu and Das Sarma[7] calculated the BGR neglecting the hole population and considering an electron plasma confined in the lowest conduction subband only. Tanatar[9] studied the

BGR in a Q1D electron-hole plasma by employing the quasi static approximation. Campos Degani and Hipolito[18] presented exchange and correlation effects in a Q1D gas using the self-consistent field method proposed by Singwi *et. al.*[19]

In low dimensional structures most often made of polar compound semiconductor materials, one has the additional complication of the long-range Fröhlich interaction between the charge carriers and the LO-phonons which also contribute to the renormalization processes. As the relevant energy scales in the problem, namely electron and hole Fermi energies, the dynamical plasma frequencies, and the LO-phonon energy become comparable, one faces an entangled many-body problem of electrons, holes, plasmons and LO-phonons, where electron-electron and electron-phonon interactions should be treated on equal footing. These polaronic renormalization effects have been subject of some recent studies.[20–22]

Despite these intense theoretical efforts, recent experimental studies reflect the fact that the BGR is still a controversial issue.[24] Theoretical results usually predict rather large band-gap shrinkage (about $\sim$ 20meV).[7,9] Even though there is general consensus about the reduction of BGR in low dimensional systems, quantitative assessment of the density dependence of the BGR is still a subject of debate.

In this chapter, the many-body theoretical formalism of the subband renormalization will be given. Our main contribution here is to extend it to a multisubband formalism, and present explicit results. As indicated before, renormalization of the band structure is associated with interaction effects in the electron-hole plasma. Basically, we have to calculate the "renormalized" quasi-particle energy, which consists of the noninteracting particle energy and the interaction energy. The interaction energy is given by the "self-energy" of the particle. Hence, the renormalization of the subband is equal to the real part of the self energy of the particle (electron, hole) in that subband. For an electron-hole system this can be formulated as

$$\Delta_i = \mathrm{Re}\left[\Sigma_{ii}^{(e)}\right] + \mathrm{Re}\left[\Sigma_{ii}^{(h)}\right] \tag{2.1}$$

where Δ_i denotes the renormalization of the ith subband.

This chapter is organized as follows: We first choose the confinement potential which models the wire, and obtain the corresponding effective Coulomb interaction matrix to be used. Then the main framework of our calculations, namely the self energy will be given. We use the so-called GW approximation[25,26] in calculating self-energy. Screening properties are described via the matrix dielectric function within the random-phase approximation (RPA). Using the effective Coulomb interaction matrix and the matrix dielectric function we construct the screened interaction matrix, which is the main ingredient (the "W" of the GW approximation) in the self energy. Finally, the explicit form of the self energy within the dynamical random-phase approximation and the quasi-static approximation employed to the screening function will be presented. The relevant parameters that affect the renormalization are the $e-h$ plasma density, the width of the wire, and the temperature. We discuss in detail the dependence on these parameters. Next, the electron–LO-phonon coupling and its effect on the renormalization process will be considered. Finally, we discuss the so-called vertex corrections that go beyond the random-phase approximation. These corrections are expected to improve the RPA result in the low density regime, where correlations are accounted for more accurately.

It might be convenient to indicate the "hidden" but crucial approximations simplifying the model here: The electron-hole gas consists of only one kind of electrons and holes with isotropic, parabolic dispersion and it is assumed to exist in a direct gap semiconductor. Thus, most of the band-structure complications of the valence subbands are neglected, and the band shifts are assumed to be rigid. This should be an adequate approximation for calculating the band-edge renormalization. Similarly, the effective mass approximation is expected to hold under the experimental conditions.

2.1 Confinement Potential and the Effective Coulomb Interaction Matrix

2.1.1 The Confinement Potential (Quantum Wire Model)

The subband structure of a quasi-one-dimensional system is determined by the confinement potential. Optical spectroscopy of quantum well wires (QWW) reflects two different confinement regimes depending on the actual size of the quantum wire. In the weak confinement regime (i.e. when the confinement is larger than $\sim a_0$ where a_0 is the exciton Bohr radius) the optical response of the QWW is dominated by the quantization of the center of mass motion of the exciton. In this case, the wide lateral potential of the large wire does not influence the electron and hole envelope functions. The main effect of the lateral boundaries is to confine the envelope function of the exciton as a whole. In the strong quantization regime, the confinement effects modify the single particle states. Experimental studies show that one has to fabricate very narrow QWWs (below 50 nm) in order to obtain real 1D quantization.[27] Our work will be restricted to this regime.

For theoretical formulation, we choose our model wire as a circular cylinder of radius R_0 with an infinite potential barrier at $r = R_0$. The envelope functions of electrons and holes in the r plane can be calculated using the Schrödinger equation in polar coordinates:

$$-\frac{\hbar^2}{2m}\left(\frac{1}{r}\frac{\partial}{\partial r}\frac{r}{m}\frac{\partial}{\partial r}+\frac{1}{r^2}\frac{\partial^2}{\partial\phi^2}\right)\zeta(r,\phi)=[E-V(r,\phi)]\,\zeta(r,\phi), \tag{2.2}$$

with,

$$V(r)=\begin{cases}0, & r<R_0\\ \infty, & r\geq R_0\end{cases} \tag{2.3}$$

The envelope functions are given in terms of Bessel functions as

$$\zeta_{nl}(r,\phi)=\frac{1}{(\pi R_0^2)^{-\frac{1}{2}}}\left[\frac{J_n(j_{nl}\frac{r}{R_0})}{J_{n+1}(j_{nl})}\right]e^{\pm in\phi}, \tag{2.4}$$

with the indices $n = 0, 1, 2, ...$ and $l = 1, 2, ...$ J_n is the Bessel function of order n and j_{nl} is its lth zero. The energy levels are

$$E_{nl} = \frac{\hbar^2 j_{nl}^2}{2mR_0^2}. \tag{2.5}$$

Other geometrical models used in the literature are rectangular and parabolic confinements. From electrodynamics point of view, the presence of the electrons and holes should be taken into account when calculating the effective potential. This amounts to a numerical solution of the Schrödinger equation coupled to the Poisson equation, which has been considered in some studies[28,29] concerning the self consistent electronic subband structure of a quantum wire.

2.1.2 Effective Coulomb Interaction Matrix

For a system with cylindrical symmetry, the interaction potential between an electron at r and an electron at r' is given by

$$V(r, r', q) = \frac{2e^2}{\varepsilon_0} K_0 \left(q \left| r - r' \right| \right), \tag{2.6}$$

where K_0 is the modified Bessel function. ε_0 is the static dielectric constant, and e denotes the electronic charge. The confinement potential modifies the Coulomb interaction by weighing it with the wave function and this is represented by a form factor. For our model we have

$$V_{klmn}(q) = \frac{2e^2}{\epsilon_0} F_{klmn}(q), \tag{2.7}$$

with the form factor,

$$F_{klmn}(q) = \int dr \int dr' \, \zeta_k(r) \zeta_l(r') K_0 \left(q \left| r - r' \right| \right) \zeta_m(r') \zeta_n(r). \tag{2.8}$$

The above matrix element can be interpreted as the scattering of two carriers from initial subbands k, l into subbands m, n, respectively. Consequently, V_{1111} is

an intra-subband interaction with all carriers remaining in the first subband, V_{1221} describes the scattering of two carriers in first and second subbands respectively, where no inter-subband transitions are induced, and V_{1122} is an inter-subband interaction in which both carriers are scattered from the first subband to the second subband. Interactions that couple inter-subband and intra-subband modes (e.g. V_{1112},V_{1222}) are not allowed in the symmetric confinement, due to the definite parity of the envelope functions. This fact is formulated by the following identity:

$$F_{klmn} = 0 \qquad \text{if } k+l+m+n = \text{odd}, \tag{2.9}$$

and the form factor remains the same under all possible permutations of first and second pair of indices among themselves.

The form factor integral has, to our knowledge, no analytical form. Gold and Ghazali[30] presented analytical results for the form factor by employing approximate wavefunctions for ground state and first excited state (irrelevant quantum numbers are suppressed),

$$\zeta_1(r) = \sqrt{\frac{3}{\pi R_0^2}}\left(1 - \frac{r^2}{R_0^2}\right), \qquad \zeta_2(r) = \sqrt{\frac{12}{\pi R_0^2}}\left(\frac{r}{R_0} - \frac{r^3}{R_0^3}\right)e^{\pm i\phi}, \quad r < R_0, \tag{2.10}$$

with the corresponding subband energies (in Rydberg),

$$E_1 = 6\left(\frac{a_B^*}{R_0}\right)^2, \qquad E_2 = 16\left(\frac{a_B^*}{R_0}\right)^2, \tag{2.11}$$

where a_B^* denotes the excitonic Bohr radius. We refer the reader to the reference[30] for the details of the calculation and cite the matrix elements of the form factor relevant to our formulation:

$$F_{1111} = \frac{2304}{x^6}\left[\frac{1}{6} - \frac{x^2}{96} + \frac{x^4}{640} - I_3(x)K_3(x)\right], \tag{2.12}$$

$$F_{1212} = \frac{18432}{x^6}\left[\frac{1}{8} - \frac{x^2}{240} + \frac{x^4}{3840} - K_4(x)I_4(x)\right], \tag{2.13}$$

$$F_{1122} = \frac{9216}{x^6}\left[\frac{1}{24} - \frac{x^2}{960} + \frac{x^4}{3840} - K_3(x)\left(I_3(x) - \frac{6}{x}I_4(x)\right)\right], \tag{2.14}$$

$$F_{2222} = \frac{36864}{x^6}\left[\frac{3}{2x^2} + \frac{1}{15} - \frac{x^2}{960} + \frac{x^4}{13440} - \left(I_3(x) - \frac{6}{x}I_4(x)\right)\left(K_3(x) + \frac{6}{x}K_4(x)\right)\right], \tag{2.15}$$

where $x = qR_0$, and $I_n(x)$ and $K_n(x)$ denote modified Bessel functions of the first and the second kind, respectively. The following asymptotic expressions are useful for numerical purposes

$$F_{1111}(qR_0 \ll 1) = -\left[\ln\left[\tfrac{qR_0}{2}\right]\left[1 + \tfrac{1}{8}(qR_0)^2 + \tfrac{9}{2^85}(qR_0)^4 + \tfrac{11}{2^{10}3^25}(qR_0)^6 + \cdots\right] - \tfrac{73}{120} + \varsigma - \tfrac{1}{8}(qR_0)^2(\tfrac{1949}{1680} - \varsigma) + \cdots\right] \tag{2.16}$$

$$F_{1122}(qR_0 \ll 1) = 0.43\left[-\ln\left[\frac{qR_0}{2}\right]\left[2.23 + 1.2(qR_0)^2\right] - 0.46(qR_0)\right] \tag{2.17}$$

$$F_{1212}(qR_0 \ll 1) = \frac{4}{7}\left(1 - 0.6(qR_0)^2 + 1.66(qR_0)^4\right) \tag{2.18}$$

$$F_{2222}(qR_0 \ll 1) = -\left[\ln\left[\frac{qR_0}{2}\right]\left[1 + \frac{1}{5}(qR_0)^2 + \cdots\right] + \varsigma - \frac{617}{1680} - (qR_0)^2\left(\frac{247}{3360} - \varsigma/5\right) + \cdots\right] \tag{2.19}$$

where $\varsigma = 0.577\ldots$ Euler's constant.

The effective Coulomb interaction is plotted in Fig.2.1 for a wire radius of $R_0 = 100$ Å. V_{1212} is a weak interaction and approaches a constant value as $qR_0 \to 0$, as can be seen from the asymptotic expression, whereas other interaction elements obey the usual logarithmic behavior for the Coulomb interaction in 1D.

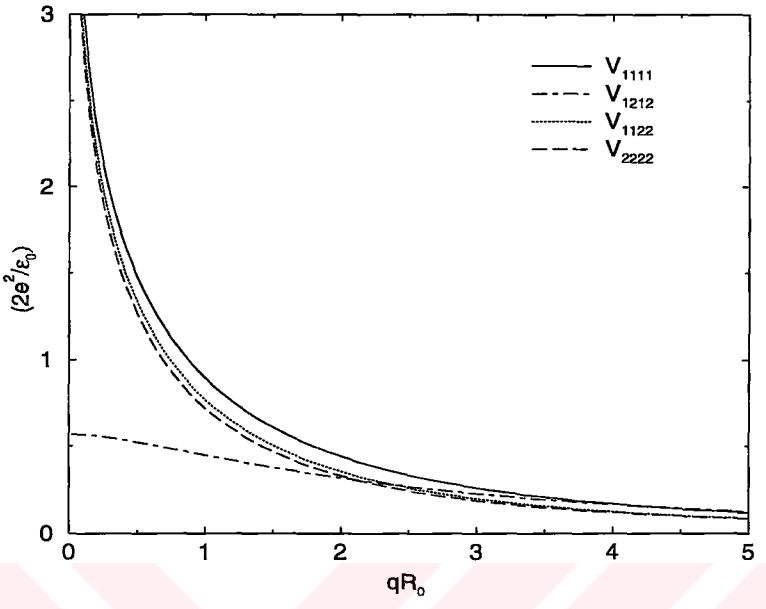

Figure 2.1: The effective Coulomb interaction matrix elements as a function of qR_0.

2.2 The electron(hole) self-energy $\Sigma(k,\omega)$ within the *GW* approximation

Generally, it is not possible to calculate $\Sigma(k,\omega)$ exactly for interacting systems, and one must resort to various approximation schemes. In particular, self-energy of the Tomonaga-Luttinger model in one dimension can be calculated exactly.[5,6] However, the connection between the exactly-solvable but artificial Tomonaga-Luttinger model and real semiconductor quantum wires is somewhat tenuous, and calculations based on more realistic models are required to make comparison with experiments. We follow the formulation developed by Hu and Das Sarma[7] for the self-energy of electrons in a quantum wire. In their model, the electrons (holes) have a parabolic dispersion in the propagation direction of the wire, and the electrons (holes) interact via exact Coulomb interaction. Unfortunately, with these assumptions, the problem can no longer be solved exactly. Hu and Das Sarma employed the *GW* approximation to calculate the self-energy,[26] where the Green's function is dressed by the dynamically screened Coulomb interaction,

which is calculated within the random-phase approximation (RPA). The Feynman diagrams for the Dyson's equation of the screened interaction and the self-energy in this approximation are shown in Fig.s 2.2(a) and 2.2(b).[7,31]

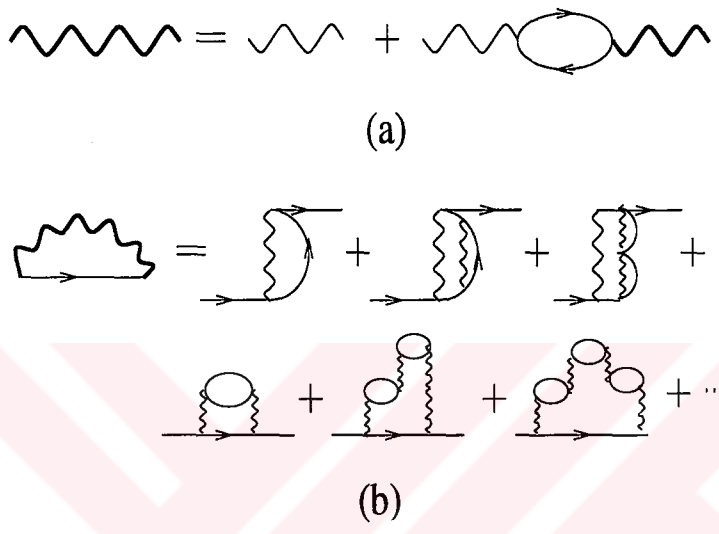

Figure 2.2: (a) Dyson's equation for the screened interaction, within the RPA. (b) Electron (hole) self-energy in leading order in the effective dynamical screened Coulomb interaction.
In figure (a), the thin wavy line is the bare Coulomb interaction, the ellipse denotes the electron-hole polarization bubble. In figure (b), the straight line denotes the bare Green's function and the thick wavy line denotes the dynamically screened interaction. Right hand side shows the terms present in the RPA

Here, we outline the multisubband formalism which was also described briefly by Hu and Das Sarma.[7] Basically, for extending the single subband formalism to the multisubband one, the functions and equations will be recast into matrix form.

The Green's function for the interacting electron-hole system obeys Dyson's equation, which we write formally in matrix form below (k and ω denote the wavevector and frequency, respectively):

$$\tilde{G}(k,\omega) = \widetilde{G^0}(k,\omega) + \widetilde{G^0}(k,\omega)\tilde{\Sigma}(k,\omega)\tilde{G}(k,\omega). \tag{2.20}$$

Here, $\widetilde{G^0}(k,\omega)$ is the noninteracting Green's function, and $\tilde{\Sigma}(k,\omega)$ is the self-energy, which includes all (i.e. infinite number of) interaction terms. In the weak coupling case (which corresponds to the high density limit for the electronic system), one can expand the self-energy in a perturbation series. In particular, the GW-approximation uses the leading term in this expansion. The explicit form of noninteracting Green function G^0_{ij} is

$$G^0_{ll'}(k,\omega) = \frac{\delta_{ll'}}{\omega - \xi_k^{(l')}}, \tag{2.21}$$

where $\xi_k^{(l')} = \frac{k^2}{2m} + E_{l'} - \mu$ is the kinetic energy at subband l' relative to the chemical potential μ. Solving the Dyson's equation gives

$$\tilde{G} = \left[\left(\widetilde{G^0}\right)^{-1} - \tilde{\Sigma}\right]^{-1}. \tag{2.22}$$

The quasiparticle energies are then given by the poles of $\tilde{G}$ i.e. at the frequencies such that $\det\left[\left(\widetilde{G^0}\right)^{-1} - \tilde{\Sigma}\right] = 0$.

The self energy in the GW approximation[33] which is attached to external electron (hole) lines from subband i and j is given by

$$\Sigma^{\lambda}_{ij}(k,\omega) = i\sum_{l} 2k_BT \sum_{\omega_m>0} \int \frac{dq}{2\pi} W_{illj}(q,\omega_m)\, G^0_{ll}(k+q,\omega+\omega_m), \tag{2.23}$$

where the first sum is over the subbands ($l = 1, 2$) , and the second sum represents the sequence of Matsubara frequencies $\omega_m = 2m\pi k_BT$, with $m = 0, 1, 2, \ldots$ W_{ijln} is the screened interaction matrix element between scattering states $i \to j$, and $l \to n$. Eqn. 2.23 is the main result of the subband renormalization problem. Dyson's equation for the screened interaction for the random-phase approximation is (see Fig. 2.2(a) for the diagrammatic representation)

$$\widetilde{W} = \tilde{V} + \tilde{V}\tilde{P}\widetilde{W}, \tag{2.24}$$

where $\tilde{P}$ is the bare polarizability function matrix (in RPA). This equation can

be solved by introducing the dielectric matrix

$$\widetilde{\varepsilon} = \widetilde{1} - \widetilde{V}\widetilde{P}, \tag{2.25}$$

and the result is

$$\widetilde{W} = \widetilde{\varepsilon}^{-1}\widetilde{V}. \tag{2.26}$$

Eqn. 2.26 defines the screened interaction matrix.

2.3 The Dielectric Function

Screening is the response of a charged many-body system to an electric field in a way that will cancel the field strength at large distances. Our concern here is the Coulomb interaction between two charges, in the presence of an electron hole plasma. The dielectric function carries all the wavevector and frequency dependence information of the screening in the system. The full derivation of the dielectric function is beyond our intentions, hence only the main features clarifying to the random-phase approximation are presented below.

The definition of the dielectric function in the interaction representation is given by[31]

$$\frac{1}{\varepsilon(q,i\omega)} = 1 - V(q)\int_0^\beta d\tau\, e^{i\omega\tau}\frac{\left\langle T_\tau \widehat{S}(\beta)\widehat{\rho}(q,\tau)\widehat{\rho}(-q,0)\right\rangle}{\langle S(\beta)\rangle}, \tag{2.27}$$

The function $\varepsilon(q,\omega)$ is the retarded function obtained from $\varepsilon(q,i\omega)$ by the analytical continuation $i\omega \to \omega + i\delta$. In Eqn.2.27, $V(q)$ denotes the bare Coulomb interaction, $\langle T_\tau \rho(q,\tau)\rho(-q,0)\rangle$ is the density-density correlation function. Here,

$$\rho(q,\tau) = e^{\tau H_0}\left[\sum_{p,\sigma} c^\dagger_{p+q,\sigma}c_{p,\sigma}\right]e^{-\tau H_0}, \tag{2.28}$$

is the density operator in the Heisenberg picture. The Hamiltonian of the noninteracting system is given by $H_0 = \sum_{p,\sigma}\xi_p c^\dagger_{p,\sigma}c_{p\sigma}$. $S(\beta)$ is the S-matrix which governs the evolution of the system from noninteracting to interacting

case. The exact evaluation of this correlation function may be written as

$$-\int_0^\beta d\tau\, e^{i\omega\tau}\,\langle T_\tau \rho(q,\tau)\rho(-q,0)\rangle = \frac{P(q,i\omega)}{1-V(q)P(q,i\omega)}, \tag{2.29}$$

where $P(q,i\omega)$ denotes the polarization function. The polarization function consists of summing of all "different" polarization diagrams arising from the expansion of the S-matrix. This can be written as an expansion $P = P^{(1)} + P^{(2)} + \cdots$ The random-phase approximation approximates the exact polarization diagram by its first term, which is $P^{(1)}(q,i\omega)$ (the polarization bubble in Fig. 2.2(b)). Thus, the corresponding RPA dielectric function is

$$\frac{1}{\varepsilon_{RPA}} = 1 + \frac{V(q)P^{(1)}}{1-V(q)P^{(1)}}, \tag{2.30}$$

which gives $\varepsilon_{RPA} = 1 - V(q)P^{(1)}(q,i\omega)$. This derivation makes clear the approximate nature of the RPA. The total polarization operator $P(q,i\omega)$ has an infinite number of terms, while the RPA retains one. The RPA dielectric function was originally derived by Lindhard for a 3D electron gas.[36]

The RPA polarization function can be evaluated as

$$\begin{aligned} P^{(1)}(q,i\omega) &= -\int_0^\beta d\tau\, e^{i\omega\tau}\,\langle T_\tau \rho(q,\tau)\rho(-q,0)\rangle \\ &= \sum_k \frac{n_F(\xi_{k+q}) - n_F(\xi_k)}{\xi_{k+q} - \xi_k - i\omega} \end{aligned} \tag{2.31}$$

where $n_F(\xi_k)$ denotes the Fermi distribution function.

In our model, the quantum wire is an intrinsic semiconductor, having equal electron and hole density. Thus, we can treat the screening by electrons and holes on an equal footing and write the total RPA polarizability as a sum of individual polarizability functions

$$P^{(1)} = P_e^{(1)} + P_h^{(1)}. \tag{2.32}$$

In the case of doped n- type and p- type semiconductors, screening by electrons and holes should be considered separately.

2.3.1 The Matrix Polarizability Function $\Pi_{ll'}(q,\omega)$

In Eqn. 2.25, the components of the RPA polarizability function matrix are given by

$$P_{ijll'}(q,\omega) = \delta_{ij}\delta_{ll'}\Pi_{ll'}(q,\omega). \tag{2.33}$$

Here, $\Pi_{ll'}$ denotes the multisubband generalization of $P^{(1)}$ (Eqn. 2.31)

$$\Pi_{ll'}(q,\omega) = 2\int \frac{dk}{2\pi}\frac{n_F\left(\xi_{k+q}^{(l)}\right) - n_F\left(\xi_k^{(l')}\right)}{\xi_{k+q}^{(l)} - \xi_k^{(l')} - \omega - i0^+}, \tag{2.34}$$

where $\xi_k^{(l)} = \frac{k^2}{2m} + E_l - \mu$ is the kinetic energy at subband l relative to the chemical potential μ, and n_F is the Fermi function,

$$n_F(x) = \frac{1}{e^{x/T}+1}. \tag{2.35}$$

Using the Dirac identity given below, one can obtain the real and imaginary parts explicitly

$$\frac{f(z)}{z - z_0 \mp i0^+} = \mathcal{P}\left(\frac{f(z)}{z-z_0}\right) \pm i\pi f(z)(z-z_0)\,, \tag{2.36}$$

where $\mathcal{P}$ denotes the Principal value integral[38]

$$\mathrm{Re}\Pi_{ll'}(q,\omega) = 2\mathcal{P}\int_{-\infty}^{+\infty}\frac{dk}{2\pi}\left[\frac{n_F\left(\xi_k^{(l)}\right)}{\frac{kq}{m} - \frac{q^2}{2m} - \omega + \Delta E_{ll'}} - \frac{n_F\left(\xi_k^{(l')}\right)}{\frac{kq}{m} + \frac{q^2}{2m} - \omega + \Delta E_{ll'}}\right], \tag{2.37}$$

$$\mathrm{Im}\Pi_{ll'}(q,\omega) = -2\pi\int_{-\infty}^{+\infty}\frac{dk}{2\pi}\left[n_F\left(\xi_{k+q}^{(l)}\right) - n_F\left(\xi_k^{(l')}\right)\right]\,\delta\left(\frac{kq}{m} + \frac{q^2}{2m} - \omega + \Delta E_{ll'}\right). \tag{2.38}$$

where $\Delta E_{ll'} = E_l - E_{l'}$ denotes the subband separation energy.

Zero Temperature Case:

At zero temperature, $\mu = E_F$, and the Fermi function reduces to a step function,

$$\lim_{T\to 0} n_F\left(\xi_k^{(l)}\right) = \Theta\left(k_F^{(l)} - |k|\right), \tag{2.39}$$

where $k_F^{(l)} = [2m(E_F - E_l)]^{1/2}\,\Theta(E_F - E_l)$ is the Fermi wavevector for the lth subband. The integral in Eqn. 2.37 can be evaluated analytically. This gives,

$$\mathrm{Re}\Pi_{ll'}(q,\omega) = \frac{m}{\pi q}\left[\ln\left|\frac{\omega_-^{(l')} + \omega - \Delta E_{ll'}}{\omega_+^{(l')} - \omega + \Delta E_{ll'}}\right| + \ln\left|\frac{\omega_-^{(l)} - \omega + \Delta E_{ll'}}{\omega_+^{(l)} + \omega - \Delta E_{ll'}}\right|\right] \tag{2.40}$$

$$\begin{aligned}\mathrm{Im}\Pi_{ll'}(q,\omega) = &\left[\Theta\left[\omega_+^{(l')} - \omega + \Delta E_{ll'}\right]\Theta\left[\omega_-^{(l')} + \omega - \Delta E_{ll'}\right]\right. \\ &\left. - \Theta\left[\omega_+^{(l)} + \omega - \Delta E_{ll'}\right]\Theta\left[\omega_-^{(l)} - \omega + \Delta E_{ll'}\right]\right].\end{aligned} \tag{2.41}$$

where $\omega_\pm^{(l)} = \frac{k_F^{(l)} q}{m} \pm \frac{q^2}{2m}$. The matrix polarizability function [Eqn.s. 2.40 and 2.41] has following properties:

$$\Pi_{ll'}(q,\omega) = \Pi_{ll'}(-q,\omega), \tag{2.42}$$

$$\mathrm{Re}\Pi_{l'l}(q,-\omega) = \mathrm{Re}\Pi_{ll'}(q,\omega), \tag{2.43}$$

$$\mathrm{Im}\Pi_{l'l}(q,-\omega) = -\mathrm{Im}\Pi_{ll'}(q,\omega), \tag{2.44}$$

and $\Pi_{ll'}(q,\omega) = 0$ if both $E_l > E_F$ and $E_{l'} > E_F$ is valid.

Finite Temperature Case

We apply the formalism developed by Maldague[37] to obtain the finite temperature expressions starting from the zero temperature formalism. In order to evaluate Eqn. 2.37 we use the following integral representation of the Fermi function

$$n_F\left(\xi_k^{(l)}\right) = \int_0^\infty d\mu'\,\Theta\left(\mu' - \xi_k^{(l)}\right)\frac{1}{4T\cosh^2\left[\left(\mu - \mu'\right)/2T\right]}. \tag{2.45}$$

Substituting in Eqn.2.37 and performing the integral over k first, we obtain

$$\mathrm{Re}\Pi_{ll'}(q,\omega;T,\mu) = \int_0^\infty d\mu'\,\Pi_{ll'}(q,\omega;T=0.\mu'). \tag{2.46}$$

The imaginary part can be evaluated in a straightforward way to yield,

$$\mathrm{Im}\Pi_{ll'}(q,\omega;T,\mu) = \frac{m}{q}\left[n_F\left(a_+^{(l)}\right) - n_F\left(a_-^{(l')}\right)\right], \tag{2.47}$$

where,

$$a_{\pm}^{(l)} = \left[\frac{m}{q}\left(\omega + \Delta E_{ll'} \pm \frac{q^2}{2m}\right)\right]^2 + E_l - \mu. \tag{2.48}$$

2.4 Screened Interaction Matrix $\widetilde{W}(q,\omega)$

We can now construct the screened interaction matrix defined by Eqn. 2.26. Using Eqn. 2.25 the explicit form of the dielectric matrix is

$$\tilde{\varepsilon} = \begin{bmatrix} & (11) & (22) & (12) & (21) \\ (11) & 1 - V_{1111}\Pi_{11} & -V_{1122}\Pi_{22} & 0 & 0 \\ (22) & -V_{1122}\Pi_{11} & 1 - V_{2222}\Pi_{22} & 0 & 0 \\ (12) & 0 & 0 & 1 - V_{1212}\Pi_{12} & 1 - V_{1212}\Pi_{12} \\ (21) & 0 & 0 & 1 - V_{1212}\Pi_{12} & 1 - V_{1212}\Pi_{12} \end{bmatrix} \tag{2.49}$$

the numbers in the small parentheses denote the subband pair indices for guidance. It is then straightforward to invert this matrix and multiply by the bare Coulomb interaction matrix $\widetilde{V}(q)$. The final result is

$$\widetilde{W} = \begin{bmatrix} & (11) & (22) & (12) & (21) \\ (11) & \frac{V_{1111}(1-V_{2222}\Pi_{22})+V_{1122}^2\Pi_{22}}{\varepsilon_{intra}} & \frac{V_{1122}}{\varepsilon_{intra}} & 0 & 0 \\ (22) & \frac{V_{1122}}{\varepsilon_{intra}} & \frac{V_{2222}(1-V_{1111}\Pi_{11})+V_{1122}^2\Pi_{11}}{\varepsilon_{intra}} & 0 & 0 \\ (12) & 0 & 0 & \frac{V_{1212}}{\varepsilon_{inter}} & \frac{V_{1212}}{\varepsilon_{inter}} \\ (21) & 0 & 0 & \frac{V_{1212}}{\varepsilon_{inter}} & \frac{V_{1212}}{\varepsilon_{inter}} \end{bmatrix} \tag{2.50}$$

In this block diagonal form, the upper block represents the intra-subband interaction, whereas the lower block includes the inter-subband terms. Similarly, the dielectric function has the intra-subband and inter-subband components given respectively as

$$\begin{aligned} \varepsilon_{intra}(q,\omega) = [1 - V_{1111}(q)\Pi_{11}(q,\omega)]\,[1 - V_{2222}(q)\Pi_{22}(q,\omega)] \\ -V_{1122}^2(q)\Pi_{11}(q,\omega)\Pi_{22}(q,\omega), \end{aligned} \tag{2.51}$$

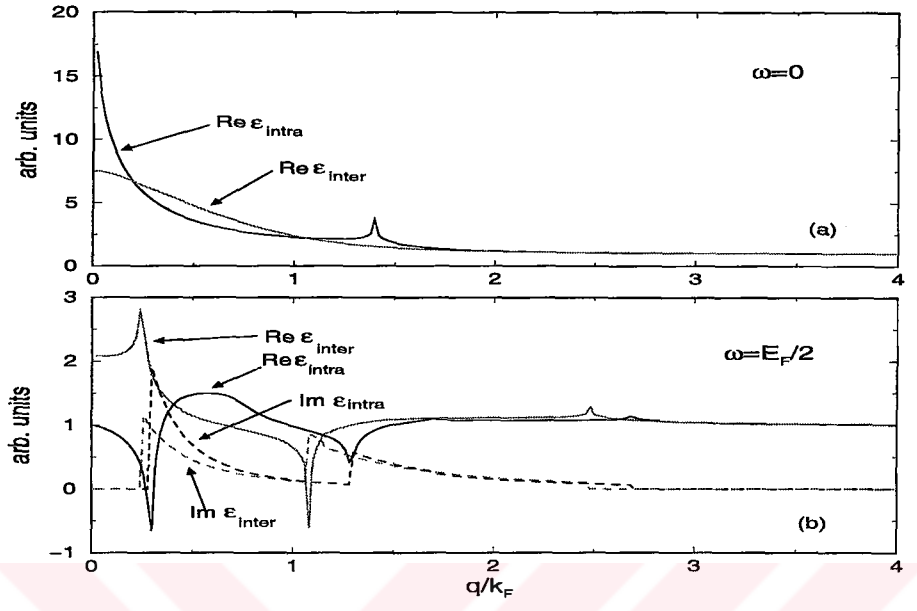

Figure 2.3: The intra- and inter-subband dielectric functions as a function of q for (a) $\omega = 0$, and (b) $\omega = E_F/2$, respectively.
The dark (light) lines show the intra (inter)-subband dielectric functions. Solid lines denote the real part, dashed lines denote the imaginary part. Other parameters are: $N = 10^6\, cm^{-1}$, $T = 0\, K$.

$$\varepsilon_{inter}(q,\omega) = 1 - V_{1212}(q)\left[\Pi_{12}(q,\omega) + \Pi_{21}(q,\omega)\right]. \tag{2.52}$$

In Fig.2.3, the zero temperature inter-subband and intra-subband dielectric functions are plotted as a function of q/k_F for $\omega = 0$ (top) and $\omega = E_F/2$ (bottom), respectively. Dielectric function is unitless. For $\omega = 0$, the imaginary parts of both dielectric functions vanish. As q goes to zero, the divergent behavior of the Coulomb matrix elements dominate in the real part of ε_{intra}. The peak on the Reε_{intra} is due to the logarithmic singularity in the polarizability functions.

In Fig.2.3(b), the ω points where the intra (inter)-subband dielectric function vanish correspond to the intra (inter)-subband plasmon modes for given ω. The spectrum of these collective excitations have been investigated by Hwang and Das Sarma.[32]

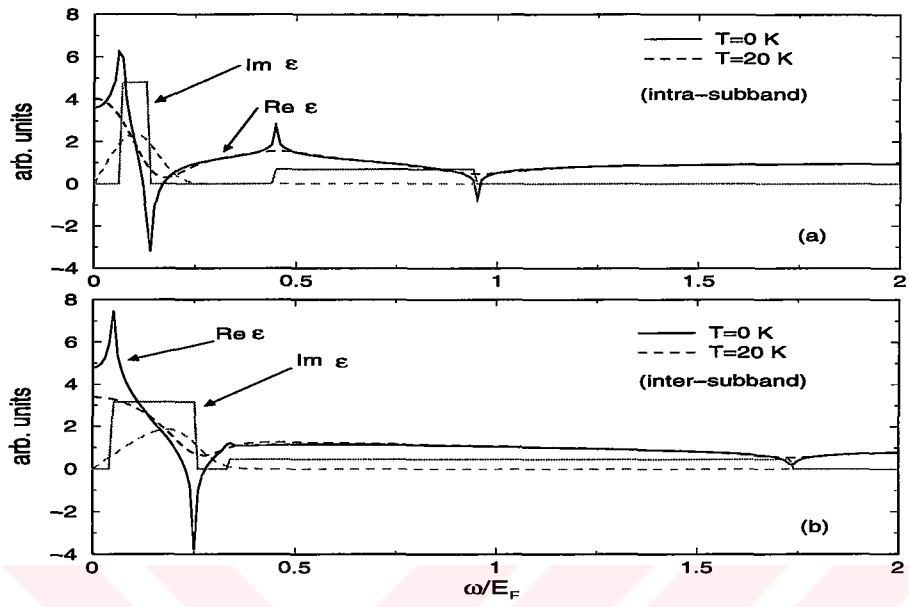

Figure 2.4: The intra-subband and inter-subband dielectric functions at $q = k_F/2$ as a function of scaled frequency.
The dark (light) lines show the real (imaginary) parts of the dielectric functions. Solid lines are for $T = 0K$, dashed lines are for $T = 20K$. Plasma density is taken as $N = 10^6\, cm^{-1}$.

In Fig.2.4 we plot this time the ω-dependence of the intra- and inter-subband dielectric functions for $q = k_F/2$. This figure gives a comparison of zero temperature and finite temperature behavior as well. Basically, finite temperature smears out the sharp features of the polarization functions.

2.5 Screened Exchange and Coulomb-Hole Decomposition of $\Sigma(k, \omega)$

The self-energy expression (Eqn. 2.23) may be decomposed into parts which have physical meaning. One possible decomposition divides the self-energy into a screened exchange term and a Coulomb-hole term:[51]

$$\Sigma_{ii} = \Sigma_{ii}^{(sx)} + \Sigma_{ii}^{(Ch)}. \tag{2.53}$$

The screened exchange term is given by

$$\Sigma_{ii}^{(sx)}(k,z) = -\sum_l \int \frac{dq}{2\pi} W_{illi}\left(q, \xi_{k+q}^{(l)} - z\right) n_F\left(\xi_{k+q}^{(l)}\right). \tag{2.54}$$

which differs from the simple exchange term by the screened interaction. Due to the Fermi distribution function, it strongly depends on occupation. Correlation energy is described by the so-called Coulomb-hole part. The name comes from the depletion shell (a "hole") around a charged particle due to the repulsive Coulomb interaction among similar charges, which leads to a reduction in quasiparticle energy. The Coulomb-hole part is further decomposed into *line* and *pole* terms,[31]

$$\Sigma_{ii}^{(Ch)}(k,z) = -\sum_l \int \frac{dq}{2\pi} 2T \sum_{\omega_n} \frac{\left(z - \xi_{k+q}^{(l)}\right)}{\omega_n^2 + \left(z - \xi_{k+q}^{(l)}\right)^2} \left[W_{illi}(q, i\omega_n) - V_{illi}(q)\right]$$
$$-\sum_l \int \frac{dq}{2\pi} \left[W_{illi}\left(q, \xi_{k+q}^{(l)} - z\right) - V_{illi}(q)\right] n_B\left(\xi_{k+q}^{(l)} - z\right). \tag{2.55}$$

Summation over Matsubara boson frequencies $i\omega_n = i2\pi nT$, $n = 0, 1, 2...$ is due to finite temperature formalism. The line contribution is pure real because $\widetilde{W}(q, -i\omega_n) = \widetilde{W}^*(q, i\omega_n)$ hence the only contribution to the imaginary part of $\Sigma_{ii}(k,\omega)$ comes from the pole part. n_B and n_F denote the Bose and Fermi distribution functions, respectively.

Equations 2.54, 2.55 give the full frequency, wavevector, and temperature dependent self-energy in the GW approximation with the RPA dielectric function. The retarded self-energy is obtained by setting $z \to \omega + i0^+$. For the subband renormalization, we evaluate the real part of the retarded self-energy at the relevant subband edge (λ denotes carrier type, i.e., electron, hole),

$$\Delta_i = \sum_\lambda \mathrm{Re}\left[\Sigma_{ii}^{(\lambda)}\left(k = 0, \omega = \xi_{k=0}^{(l)}\right)\right]. \tag{2.56}$$

At zero temperature the sequence of Matsubara frequencies becomes a continuum, and the summation is replaced by an integral over the frequency variable as $2T\sum_{\omega_n} \to \int d\omega/2\pi$. Furthermore, the Bose and Fermi frequencies reduce to step

functions. Hence the real part of the self energy contributions at zero temperature evaluated at the band-edge are given by,

$$\mathrm{Re}\Sigma_{ii}^{(sx)} = -\sum_{l} 2\int_{0}^{k_F^{(l)}} \frac{dq}{2\pi} W_{illi}(q), \tag{2.57}$$

$$\mathrm{Re}\Sigma_{ii}^{(Ch)} = \sum_{l}\int \frac{dq}{2\pi}\int \frac{d\omega'}{2\pi} \frac{\left(\xi_{k=0}^{(i)} - \xi_{q}^{(l)}\right)}{\omega'^2 + \left(\xi_{k=0}^{(i)} - \xi_{q}^{(l)}\right)^2} \left[W_{illi}(q,\omega) - V_{illi}(q)\right]$$
$$-\sum_{l}\int \frac{dq}{2\pi}\mathrm{Re}\left[\left[W_{illi}\left(q, \xi_{q}^{(l)} - \xi_{k=0}^{(i)}\right) - V_{illi}(q)\right]\right]\left[-\Theta\left(\xi_{k=0}^{(i)} - \xi_{q}^{(l)}\right)\right]. \tag{2.58}$$

2.6 The Quasi-static Approximation

The numerical cost of calculating the full frequency dependent self-energy terms is high, as it requires a summation (or an integral in $T = 0$ case) over frequencies. The quasi-static approximation[11,12]is introduced to remedy this computational cost. This approximation amounts to replacing the dielectric function by its static (i.e. $\omega = 0$) value in the final expressions. This is *different* than the simple static approximation which would arise if the screened interaction in Eqn.2.23 is replaced *a priori* by its static value. This scheme leads to serious errors in the calculation of the correlation energy, as noted in the literature.[12]

In the quasi static limit, only the fractional expression in the line term (Eqn. 2.55, first line) depends on the Matsubara frequency and that sum can be reduced to a functional form:

$$2T\sum_{\omega_n} \frac{\left(z - \xi_{k+q}^{(l)}\right)}{\omega_n^2 + \left(z - \xi_{k+q}^{(l)}\right)^2} = \frac{T}{\left(z - \xi_{k+q}^{(l)}\right)} + \frac{1}{2}\coth\left[\frac{\left(z - \xi_{k+q}^{(l)}\right)}{2T}\right], \tag{2.59}$$

where we have used the mathematical identity,[47]

$$\coth(\pi x) = \frac{1}{\pi x} + \frac{2x}{\pi}\sum_{k=1}^{\infty}\frac{1}{x^2 + k^2}. \tag{2.60}$$

Previous studies[9,12] indicate that the quasi-static approximation tends to overestimate the correlation energy. When presenting our numerical results, we shall address this point and discuss the importance of dynamical correlations.

2.7 LO-phonon interaction effects

If we include coupling of the electron-hole system to LO-phonons, the corresponding phonon interaction potential should be added to the bare Coulomb interaction. Thus we replace the bare Coulomb interaction (Eqn. 2.7) as (the subband indices are suppressed)

$$V(q) \rightarrow V_{eff}(q,\omega) = V(q) + V_{ph}(q,\omega), \tag{2.61}$$

where the general form of the phonon potential is given by

$$V_{ph}(q,\omega) = \sum_{q} |M(q)|^2 D(q,\omega,\omega_q). \tag{2.62}$$

In this equation, $|M(q)|^2$ is the squared matrix element of the interaction between the carriers and the phonons concerned, ω_q is the phonon frequency, and $D(q,\omega,\omega_q)$ the phonon propagator given by[31] $D(q,\omega,\omega_q) = 2\omega_q / \left(\omega^2 - \omega_q^2\right)$. For bulk phonons the matrix element is

$$|M(q)|^2 = V(q)\frac{\omega_q}{2}\left(1 - \frac{\epsilon_\infty}{\epsilon_0}\right), \tag{2.63}$$

and if we further assume dispersionless bulk LO-phonons, we set $\omega_q = \omega_{LO}$. This yields the final form of the effective interaction as

$$V_{eff}(q,\omega) = V(q)\left[1 + \frac{\omega_{LO}^2}{\omega^2 - \omega_{LO}^2}\left(1 - \frac{\epsilon_\infty}{\epsilon_0}\right)\right]. \tag{2.64}$$

Using the Lyddane-Sachs-Teller relation $\epsilon_0/\epsilon_\infty = \omega_{LO}^2/\omega_{TO}^2$ we can write

$$V_{eff}(q,\omega) = \frac{V(q)}{\varepsilon_{ph}(q,\omega)}, \tag{2.65}$$

where $\varepsilon_{ph}(q,\omega) = (\omega^2 - \omega_{LO}^2) / (\omega^2 - \omega_{TO}^2)$ is the phonon dielectric function which screens the bare Coulomb interaction due to electron-phonon coupling. In our previous discussion of the dielectric function, we took $V_{ph} = 0$ and employed the so-called ϵ_0 approximation, which consists of replacing the high frequency dielectric function ϵ_∞ by ϵ_0 in the Coulomb potential (Eqn. 2.7). Note that, if we resort to the LO-phonon coupling via the ε_{ph}, we must undo the ϵ_0 approximation. The rationale of the ϵ_0 approximation is that, the main effect of the high-frequency LO phonons is to screen the Coulomb interaction, which is suitably accounted for by the replacement of ϵ_∞ by ϵ_0. Das Sarma *et al.*[50] investigated the validity of the ϵ_0 approximation for the 2D and quasi-2D semiconductor quantum wells and concluded that for weakly polar materials (e.g. GaAs, InAs, Ge, Si) the phonon coupling effects are very well approximated by ϵ_0, provided that the carrier densities do not reach very high values. This is because with increasing carrier density, the Fermi energies become comparable to the LO-phonon energy which makes the ϵ_0 approximation less appropriate.

In including LO-phonons one has to subtract the phonon self-energy, which is always present and can not be detected separately by experiment. In perturbation theory, the phonon self-energy (modified to our multisubband formalism) reads

$$\Delta E_i^{(ph)} = -\left(1 - \frac{\omega_{TO}^2}{\omega_{LO}^2}\right) \frac{\omega_{LO}}{2} \sum_l \int \frac{dq}{2\pi} \frac{V_{illi}(q)}{\omega_{LO} + \xi_q^{(l)}}, \tag{2.66}$$

which should be calculated for electrons and holes and added together.

2.8 Results For The Subband Renormalization

In this section, we present the results of calculations based on GaAs material parameters, which we summarize in Table2.1. We used the scaling based on

$m_e = 0.067$	$\epsilon_0 = 13.74$	$a_0 = 119.77$ Å
$m_h = 0.457$	$\epsilon_\infty = 10.9$	$E_0 = 4.66$Ryd

Table 2.1: GaAs material parameters used in the numerical calculations.

the three dimensional excitonic Bohr radius a_0 and excitonic Rydberg E_0. Das Sarma *et.* al.[50] indicated in that in quantum well structures, a proper scaling can give a band-gap renormalization expressed in units of effective Rydberg which shows a universality, independent of the band-structure details of the material and dependent only on the electron-hole density and the well width.

Typical electron-hole plasma densities generated by photo-excitation in experiments vary between $10^4 - 10^6$ cm^{-1}. In Fig. 2.5, the chemical potential of electrons is plotted for single subband model (thin solid line) and for two-subband model (thick lines), at various temperatures. For wire radius of $R_0 = 150$ Å, the first two subbands are located at $0.67\,E_0$ and $1.71\,E_0$, respectively. At zero temperature, the second subband starts to populate around $N \sim 1.4 \times 10^6$ cm^{-1}, where the chemical potential within the two-subband model deviates from the single subband result. Increasing temperature smears the sharp change at the onset of second subband population (see the inset figure).

The second subband level (solid line) and the chemical potential at a fixed density (dashed line) are plotted as a function of wire radius in Fig.2.6. As the radius range and the density are close to experimental conditions, the two-subband model appears to be appropriate for calculating the renormalization effects.

As the formulation given in the previous sections has different aspects to compare, (e.g. single subband vs. two-subband, dynamic vs. quasi-static) a systematic presentation is appropriate. We first consider the full dynamical, zero temperature formalism and plot the subband renormalization as a function of density. Fig. 2.7 shows the results for single subband and two-subband formalisms for comparison.

The wire radius is taken to be 100 Å. At low densities, the single subband (thin solid line) and two-subband (thick solid line) formulations give nearly same

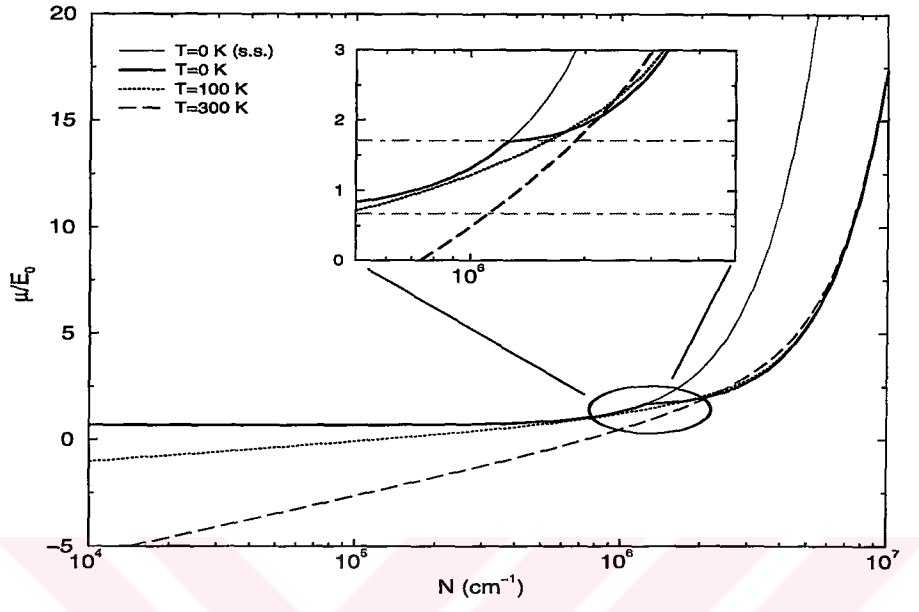

Figure 2.5: The chemical potential of electrons as a function of density Wire radius is $R_0 = 150$ Å. Thin solid line is the single subband result. Two dash-dotted lines in the inset figure denote the first and second subband levels, respectively.

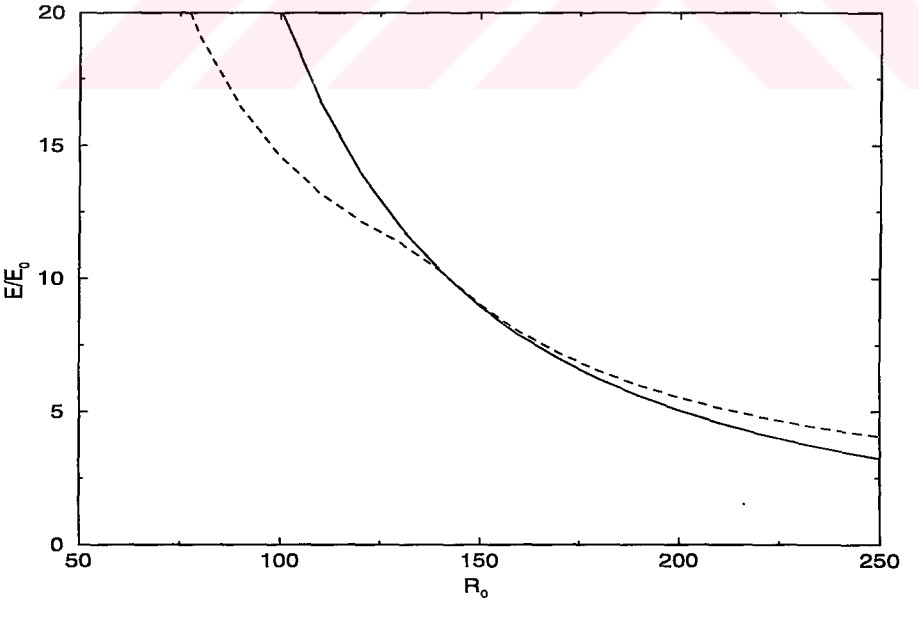

Figure 2.6: The chemical potential (dotted line) and the second subband level (solid line) at $N = 1.4 \times 10^6$ cm^{-1} as a function of wire radius.

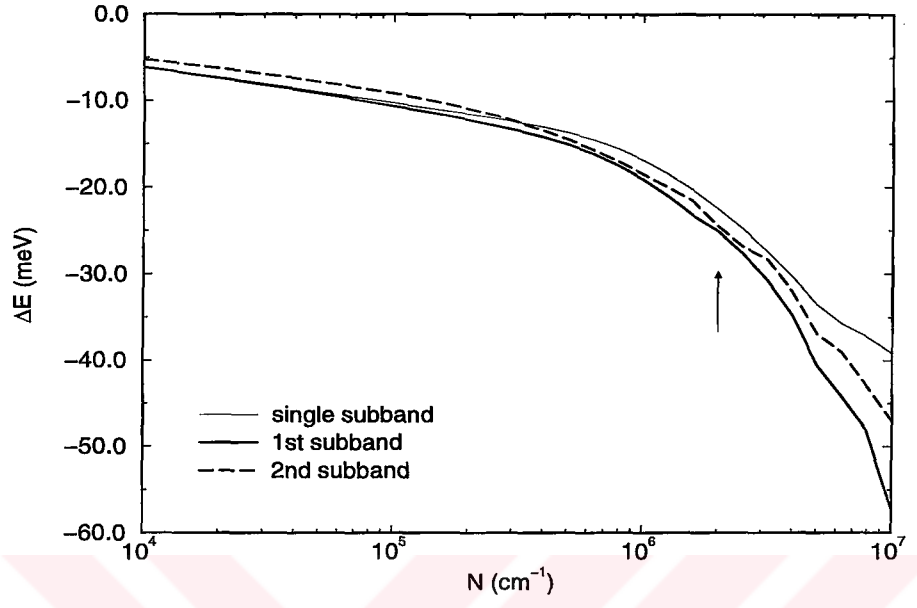

Figure 2.7: The subband renormalization as a function of density. Wire radius is $R_0 = 100$ Å. Full dynamical RPA formalism at $T = 0$ K is used. Solid (dashed) line shows the first(second) subband. The thin solid line shows the single subband result.

renormalization values, but after the population of second subband, they deviate significantly. Interestingly, the renormalization of the second subband is quite close to the first subband. Although this looks peculiar, especially when the second subband is empty, a detailed inspection of the contributions to the total renormalization seems to give a reasonable explanation. For this purpose we plot in Fig.2.8 the screened exchange and Coulomb contributions to each subband, which are given by Eqn.s 2.57, 2.58, respectively. The screened exchange depends on occupation, and the second subband is less occupied than the first one. The subband wavevector is given by

$$k_F^{(i)} = \begin{cases} \sqrt{2m(E_F - E_i}, & E_i < E_F \\ 0, & otherwise \end{cases} \tag{2.67}$$

If we write the inter-subband and intra-subband terms of the screened

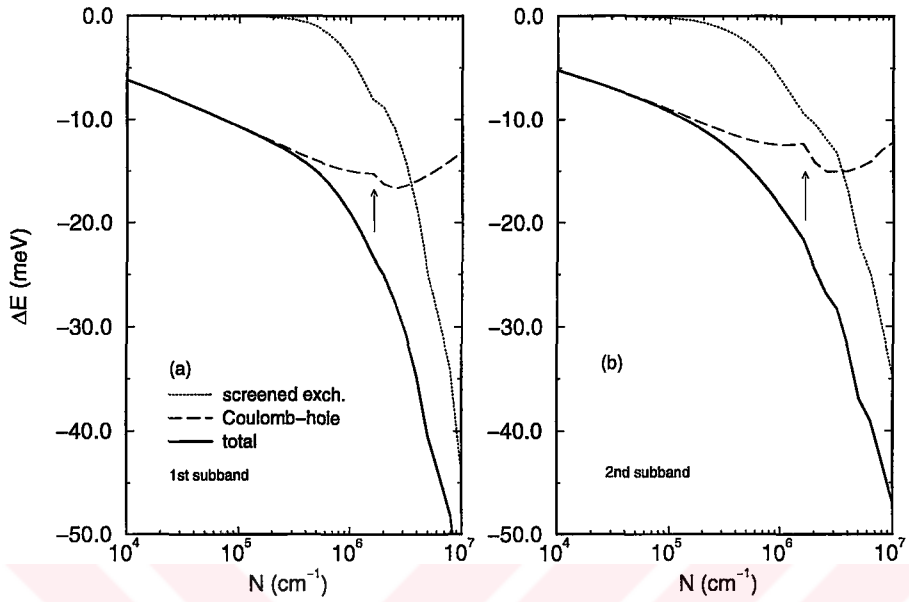

Figure 2.8: The screened exchange and Coulomb-hole contributions to the subband renormalization as a function of density.

exchange energy (Eqn. 2.57) separately,

$$\mathrm{Re}\Sigma_{ii}^{(sx)} = -2\int_0^{k_F^{(i)}} \frac{dq}{2\pi} W_{iiii}(q) - 2\int_0^{k_F^{(j)}} \frac{dq}{2\pi} W_{ijji}(q)\,, \tag{2.68}$$

it is easy to see that the intra-subband contribution is zero unless the relevant subband is occupied, but the inter-subband contribution depends on the occupation of the other subband. Hence, the second subband acquires a finite contribution from the first subband throughout the whole density range, whereas the first subband gets this contribution only after the onset of the second subband population. The inter-subband interaction is smaller than the intra-subband one, but a direct comparison of the screened interaction strengths W_{iiii} and W_{ijij} is not as trivial as in the bare Coulomb interaction matrix elements, as these screened interaction elements possess intra-subband and inter-subband plasmon poles, respectively.

The dominant contribution at low densities comes from the Coulomb-hole term, but the general behavior of the renormalization is due to screened exchange

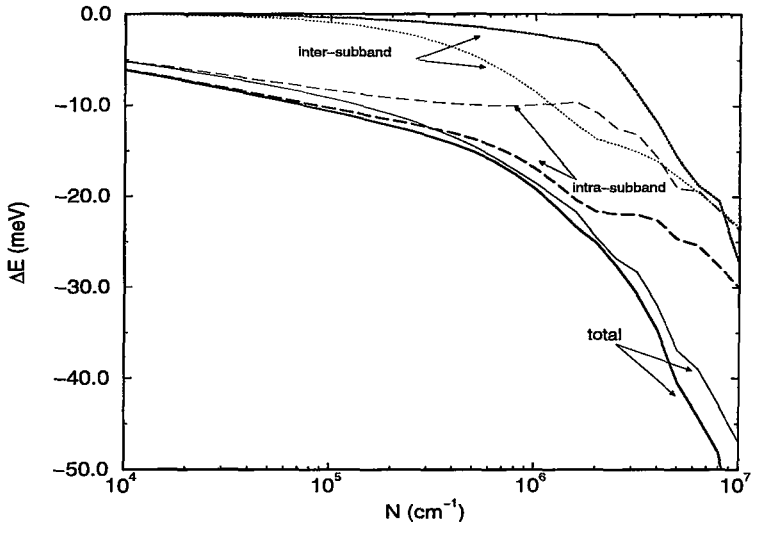

Figure 2.9: The intra-subband and inter-subband contributions to the subband renormalization as a function of density.

term. The Coulomb-hole contribution depends upon how effectively the Coulomb field of the particle is screened and is relatively insensitive to the details of the subband occupation. At zero temperature, the intra-subband term of the pole part vanishes due to the Bose factor, but for the second subband, the inter-subband term does bring a finite contribution.

Finally, we plot the inter-subband and intra-subband contributions separately. Fig. 2.9 shows these contributions along with the total renormalization. As expected, the inter-subband contributions are relatively small in the density range where the second subband is empty.

Based on the results depicted in figures 2.7 - 2.9 we conclude that a multisubband formulation gives different results compared to single subband formulation. The very presence of the second subband alters the renormalization process, and with the onset of second subband population, the inter-subband contributions become significant. On the other hand, the subband separation remains rather insensitive to the renormalization, but seem to increase at very high density ($N \sim 10^7$ cm^{-1}). The width of the wire essentially determines the dimensionality of the system, thus it affects the subband renormalization

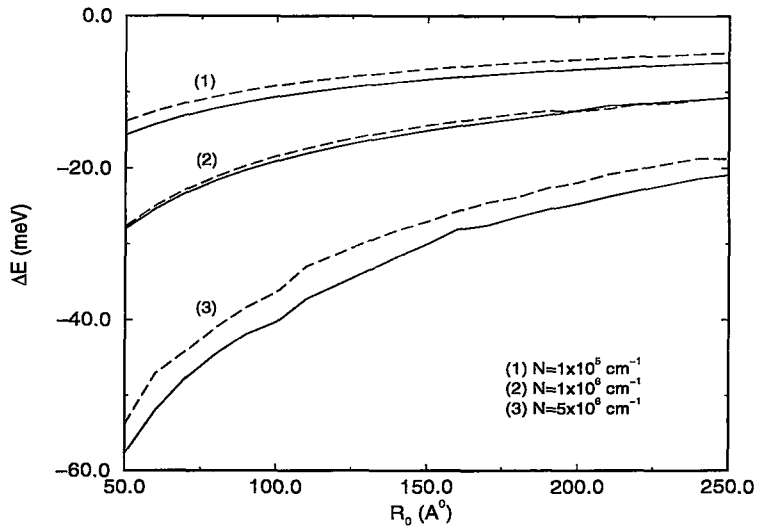

Figure 2.10: The subband renormalization as a function of wire radius at various densities. Solid (dashed) line indicates first (second) subband.

directly. Narrower confinement enhances the form factor and increases the interaction energy. Fig. 2.10 shows the wire radius dependence of the subband renormalization at different fixed plasma densities. For the top most curve, second subband remains empty throughout the given radius range, for the middle curve second subband starts to populate close to $\sim$ 200 Å, and for the lower curve second subband is always populated. For very large radii, the two-subband formulation is likely to give worse results since the subband separation is small, and more subbands get populated.

In section 2.6, we have introduced the quasi-static formulation, which is widely used in the literature. Calculations based on this approximation in higher dimensions[8] led to the conclusion that the quasi-static approximation tend to overestimate the renormalization effects. Here, we make the comparison of dynamic and quasi-static approximations for a quasi-one-dimensional system. Fig. 2.11 shows the calculated renormalization. At low densities there is a considerable difference between the two approximations. The outcome of the quasi-static approximation is consistent with that of higher dimensions: it overestimates the renormalization. With increasing density, this discrepancy

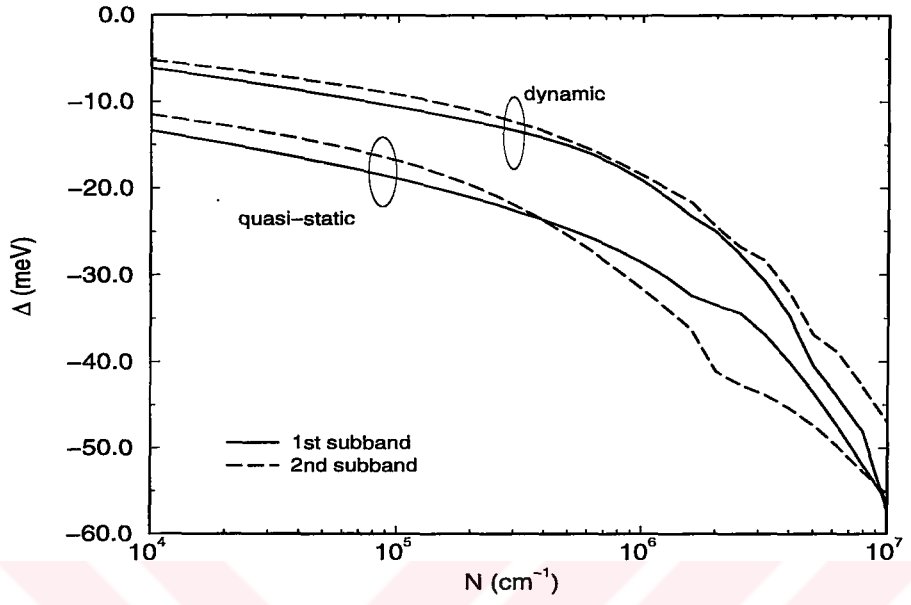

Figure 2.11: The full dynamical RPA vs. the quasi-static approximation

decreases. This reflects the importance of dynamical screening effects at low density regime.

2.8.1 Finite Temperature Effects

In general, many-body calculations in metals[33–35] have used the zero temperature formalism because the energy scales intrinsic to the problem (Fermi energy, plasmon energy, etc.) are usually much larger than the temperature T. In semiconductors, especially in artificial structures of reduced dimensionality, because of the low electron densities and large lattice dielectric constants involved, the experimental temperature can be comparable to the intrinsic energy scales of the electron-hole plasma.

For a quantum wire density of 5×10^5 cm^{-1}, the Fermi energies are of order 10 meV $\sim$ 100 K. Therefore, within the range of the plasma densities under discussion, the zero temperature formalism might be adequate for temperatures well below this value. Yet, a finite temperature formalism is needed to extend the results to room temperature ($T \sim 300$ K). For this purpose, we plot the

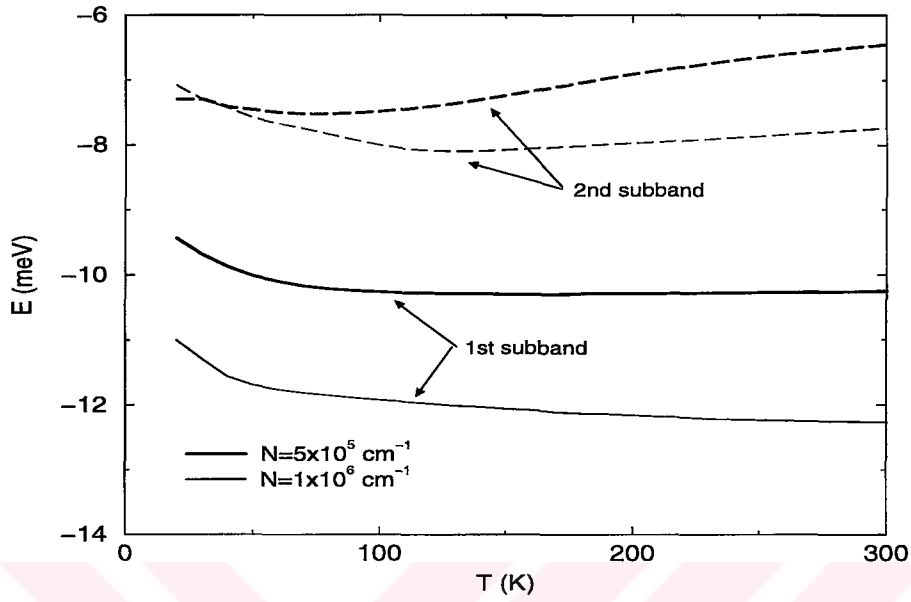

Figure 2.12: Temperature dependence of the subband renormalization.

subband renormalization as a function of temperature at two different plasma densities in Fig.2.12. Surprisingly, the subband renormalization does not depend strongly on temperature. For $N = 5 \times 10^5$ cm^{-1}, the change in the second subband renormalization is stronger. This might be due to the fact that, with increasing temperature, this subband starts to get populated, resulting in a more significant change in the renormalization. In conclusion, temperature effects are less significant in the renormalization, indicating that the characteristics of quantum wire lasers might be robust against changes in temperature of the environment.

2.9 Coupling to Bulk-LO Phonons

In section 2.7, the coupling to LO-phonons have been introduced. For weakly polar materials (e.g. GaAs, InAs, GaSb) the ϵ_0 approximation is shown to work very well for 2D quantum wells,[50] and Q1D quantum wires.[22,23] Here, we consider the coupling to bulk-LO phonons within the two-subband formalism.

In Fig. 2.13 we present the effect due coupling to LO-phonons (solid lines)

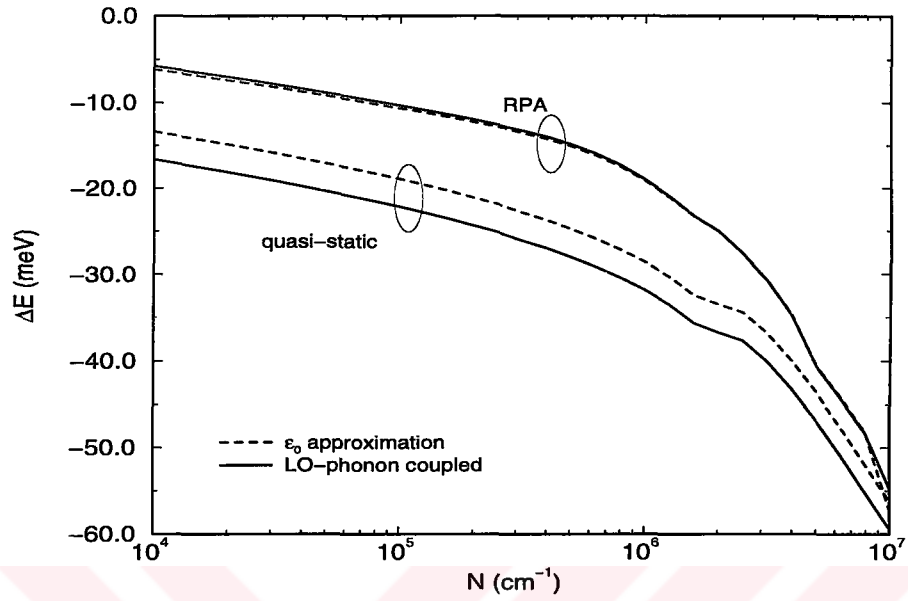

Figure 2.13: Bulk LO-phonon coupling effects

compared with ϵ_0 approximation (dashed lines) in the dynamical RPA and the quasi-static approximation for the first subband. Treating the electron-LO-phonon and electron-electron interactions on an equal footing does not affect the full dynamical result significantly, hence the ϵ_0 approximation seems to work well. The dynamical screening function of phonons further decreases the strength of the screened interaction which causes an increase in the renormalization, but then this is compensated by the subtraction of the polaronic self-energy, which brings the renormalization again close to the ϵ_0 result. The quasi-static result, however, is shifted to higher renormalization values, although the subtraction of the polaronic shift tend to reduce it. The net result is that the difference between the quasi-static result and the full RPA increases. In the high density regime different approximations merge together, smearing out the polaronic and other dynamical effects.

An interesting situation may arise when the subband separation becomes equal to the LO-phonon energy. In this case, the polaronic self-energy shows a divergent behavior. Whether this would lead to a remarkable effect in the optical spectra is yet to be studied. From experimental point of view, this requires the

production of very clean wire structures, where the subband separation can be tuned in a controllable way.

2.10 Beyond RPA: The Vertex Corrections

The random-phase approximation becomes less appropriate in low density regime. In this case other interaction diagrams that are omitted in RPA should be taken into account. The so-called vertex diagrams are one set of diagrams which couple the branches of the polarization bubble. In case of single species (only electron or hole) extending the formalism to include vertex corrections is rather straightforward: The self energy is written as

$$\Sigma(k,E) = i\int \frac{dq}{2\pi}\int \frac{d\omega}{2\pi}\frac{V(q)}{\varepsilon(q,\omega)}\gamma(q,\omega)G_0\left(|k-q|, E-\omega\right) \tag{2.69}$$

which is known as the $GW\Gamma$ approximation to the self energy.[26,34] The dielectric function is given by

$$\varepsilon(q,\omega) = 1 - V(q)\chi_0(q,\omega)\gamma(q,\omega)\,, \tag{2.70}$$

and

$$\gamma(q,\omega) = \frac{1}{1+\mathcal{G}(q)V(q)\chi_0(q,\omega)}\,, \tag{2.71}$$

where χ_0 is the noninteracting polarizability for electrons, and $\mathcal{G}(q)$ is a vertex correction given in the Hubbard approximation in the one dimensional limit by[30]

$$\mathcal{G}(q) = \frac{1}{2}\frac{V\left(\sqrt{q^2+k_F^2}\right)}{V(q)}\,. \tag{2.72}$$

The Hubbard approximation takes exchange into account and corresponds to using the Pauli hole in the calculation of the local field correction between the particles of the same kind. Coulomb correlations are omitted. Note that for $\mathcal{G}(q) = 0$, or equivalently $\gamma(q,\omega=0) = 1$, the GW approximation in RPA is

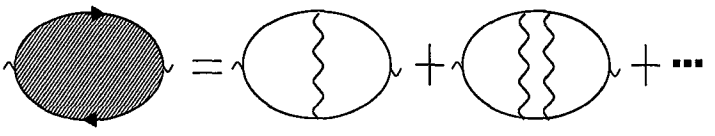

Figure 2.14: Vertex correction to the basic bubble diagram (shaded bubble). The right hand side represents the expansion in an infinite set of individual vertex lines which couple the propagators (upper and lower branches of the bubble) via the Coulomb interaction.

recovered.

Marmorkos and Das Sarma[39] have studied the many-body vertex corrections on quasiparticles of two-dimensional electron systems. They found that vertex corrections improve the RPA results, particularly at lower densities. Tanatar[9] included the vertex correction in the dielectric function only, and drew similar conclusions for the calculation of the band-gap renormalization in a quantum wire.

For a two-component (electron-hole) plasma, the vertex correction formalism is a rather formidable task. In general, we have to write the self-energy as

$$\begin{pmatrix} \Sigma_e \\ \Sigma_h \end{pmatrix} = \begin{pmatrix} W_{ee} & W_{eh} \\ W_{he} & W_{hh} \end{pmatrix} \begin{pmatrix} G_e^0 \\ G_h^0 \end{pmatrix} \tag{2.73}$$

where W_{ij} is the matrix element for the screened interaction between particles of kind i and j, G_i is the noninteracting Green function of particle of kind i. Note that, the 2×2 matrix form arising here is *not* due to multi-subband structure, but due only to the *two-component* nature of the plasma. We did not include the interaction among different species as depicted here, but it is present

within the screened interaction terms. The vertex correction for the interaction among electron and hole cannot be accounted for by the Hubbard approximation ($\mathcal{G}_{12} = 0$). One has to construct the ladder-vertex integral equations in the two-component formalism given in Eqn.2.73 which is a rather formidable task.

Chapter 3

Many-body effects on optical spectra of semiconductor quantum wires: The interplay of excitons and free carriers

In this chapter, we would like to review recent studies concerning correlation effects on optical properties of semiconductor quantum wires. Our aim is to provide some conclusions drawn in these studies and to construct a picture of how the Coulomb correlation affects optical spectra which are shaped by the excitons and the electron-hole plasma.

The many-body formalism of excitons in a degenerate electron-hole plasma is not a new subject. Correlation effects are studied within the many-body theoretical framework by the using the so called T-matrix method. This method describes multiple scattering events between electron and hole via the screened interaction. Mahan[40] has studied excitonic features in the absorption spectrum of a direct gap bulk semiconductor with a degenerate (n or p type) band. The calculations show that exciton states cause a logarithmic singularity in the absorption at the Burstein edge. This singularity is present at a moderate density of electrons and holes in the degenerate band, but it gradually disappears in the

high-density limit. Schmitt-Rink *et. al*[44] considered the many-body effects in the absorption spectra of two dimensional quantum-well structures.

On the other hand, the optical spectra of highly excited semiconductor quantum wire structures have recently attracted a great deal of experimental,[24,48,49] and theoretical[54–58] attention. At first glance, quantum wires seem to provide drastically improved performance in optical applications with respect to their three-dimensional (3D) and two-dimensional (2D) counterparts, by taking advantage of the 1D singularities that are expected in the density of states and in the optical spectra on the basis of single particle band models. However, excitonic and correlation effects are very important in low-dimensional systems, and thus, should be included in the models. For 1D systems, such effects were studied mostly within single-subband models,[59] which showed a smoothing when excitonic effects are taken into account; moreover, Coulomb correlation is found to reduce the absorption peaks above the band-edge, contrary to the well known results for 2D and 3D systems.[60] Rossi and Molinari[57] studied linear and nonlinear optical properties of realistic quantum-wire structures by considering T-shaped quantum wires and by taking the subband structure into account. Their approach is based on a set of generalized Bloch equations, which are solved within the Hartree-Fock approximation and provide the modified optical spectrum for bound and continuum states in the linear (low density) and nonlinear (high density) regimes. Their results also indicate the suppression of sharp features in the free-carrier density of states.

Before we consider the many-body theoretical formalism, let us note that a general treatment of the combined exciton–electron-hole plasma system for arbitrary density and temperature range is practically impossible. One has to concentrate on a particular region in the density-temperature phase-space, where some progress can be made by the validity of significant approximations. In the following section, we shall consider the problem of a single electron-hole pair embedded in an electron-hole plasma. This concept holds only at elevated temperatures, strictly speaking for $T \gg E_0$, where E_0 is the exciton binding energy, or at high densities, where bound states are ionized.

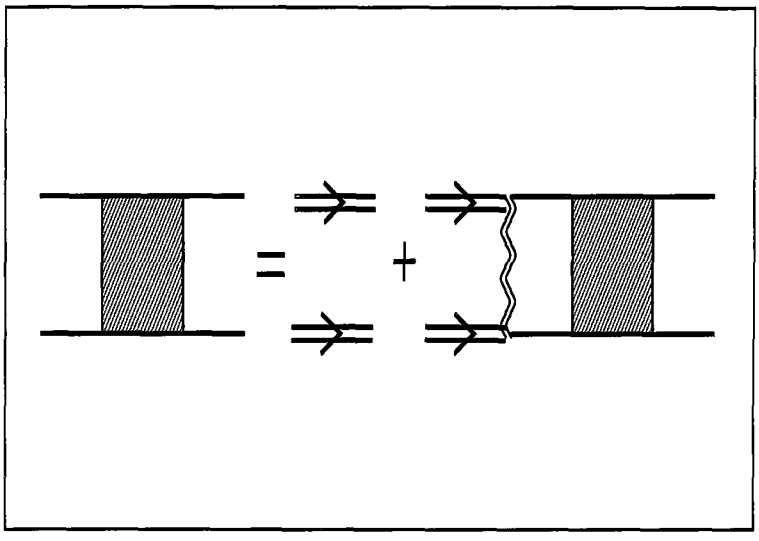

Figure 3.1: The Bethe-Salpeter equation for the $e-h$ pair propagator. Straight double line denotes the free $e-h$ propagator. Wavy line is the screened Coulomb interaction. Shaded square stands for the T-matrix, representing the multiple scattering events between electron and hole.

3.1 T-Matrix formulation

The properties of the electron-hole pair are described by the two particle propagator $G(k,k',\omega)$. Within the screened ladder approximation $G(k,k',\omega)$ obeys the Bethe-Salpeter equation (BSE), which is depicted in fig.3.1.

The shaded square represents the multiple scattering process of electron and hole, known as T-matrix. The wavy line is the screened interaction among the $e-h$ pair. In analytical language fig.3.1 reads[12]

$$G(k,k',z,\Omega) = G^0(k,k',z,\Omega) + \frac{1}{\beta}\sum_{k'',k''',z'} G^0(k,k'',z,\Omega)V_s(k''-k''',z-z') \times G(k''',k',z',\Omega)\,, \tag{3.1}$$

where

$$G^0(k,k',z,\Omega) = G_e(k,\Omega-z)G_h(-k,z)\delta_{k,k'}\,, \tag{3.2}$$

and the single particle propagator which includes the renormalized single particle

energies $E_i(k,z) = \xi_k^i + \Sigma(k,z) - \mu_i$ is given by

$$G_i(k,z) = \frac{1}{z - E_i(k,z)}. \tag{3.3}$$

In Eqn.3.1, $V_s(k-k', z-z')$ is the dynamically screened interaction between electron and hole. In some studies[58,61] the interaction potential is taken as the so-called contact potential $V(x) = a\delta(x)$ (resulting in a constant potential in q-space) with $a \sim E_0 a_0$ such that it reproduces the exciton binding energy in the limit of low density (a_0 is the exciton radius). The contact potential for identical fermions is not compatible with Pauli's exclusion principle, thus, electron-electron and hole-hole interactions are absent for the same spin. It is also noted that the screening cannot be consistently introduced within such a restricted form of the potential. Despite these drawbacks, the contact reproduces the main features of the Coulomb correlation. The reason is that, this short-range interaction may represent the Coulomb interaction in a $e-h$ plasma, where the interaction range is greatly reduced due to screening. The contact potential further enables to introduce more sophisticated schemes like the self-consistent ladder approximation (SCLA)[58] which partially recovers higher order correlations and thus extends the usual ladder approximation results to higher densities. Use of the Coulomb potential would be the natural choice, however, a full dynamical screening formalism (like the RPA) makes the formulation quite complicated. In the following, we would like to outline the formalism by Schmitt-Rink *et. al*[53] which is developed for a quantum-well system. This formalism is not full dynamical, but it is based on the statically screened Coulomb interaction in the plasmon-pole approximation.

Within the statical approximation, the renormalized single particle energies are given by

$$E_i(k) = \xi_k^i + \Sigma_i(k)\,, \tag{3.4}$$

where the $\Sigma_i(k)$ are the single-particle self-energies. In section 2.6 these are given for two-subband formalism. Here we reduce them to the single subband case and

suppress the subband index henceforth,

$$\Sigma_i(k) = \Sigma_i^{sx}(k) + \Sigma_i^{Ch}\,, \tag{3.5}$$

where the screened exchange and Coulomb-hole terms are defined as

$$\Sigma_i^{sx} = -\sum_{k'} V_s(k-k') f_i(k') \tag{3.6}$$

$$\Sigma_i^{Ch} = \frac{1}{2}\sum_{k'} [V_s(k') - V_s(k)]\,, \tag{3.7}$$

and

$$f_i(k) = \frac{1}{e^{[E_i(k)-\mu]/T}+1} \tag{3.8}$$

is the quasiparticle distribution function. Eqn. 3.1 can be written in retarded form as

$$G(k,k',\omega) = G_0(k,k',\omega) - \sum_{k'',k'''} G_0(k,k'',\omega) V_s(k''-k''') G(k''',k',\omega)\,, \tag{3.9}$$

where

$$G_0(k,k',\omega) = \frac{F(k)}{\omega + i\delta - E_e(k) - E_h(k)}\delta_{k,k'}\,. \tag{3.10}$$

The nominator is the phase-occupation factor, $F(k) = 1 - f_e(k) - f_h(k)$ which reflects the Pauli exclusion principle.

The $e-h$ pair propagator is expanded in terms of eigenfunctions of the homogeneous part of the BSE,

$$G(k,k',\omega) = \sum_n \frac{|F(k)|^{1/2}\,\phi_n^*(k)\,|F(k')|^{1/2}\,\phi_n(k')}{\omega + i\delta - E_n} \times \mathrm{sgn}(E_n - \mu)\,. \tag{3.11}$$

In the plasma state, bound states no longer exist, so that the eigenfunctions $\phi_n(k)$ are scattering states $\phi_p(k)$, classified according to the relative $e-h$ momentum p. The $e-h$ pair energies are $E(p) = E_e(p) + E_h(p)$. $\phi_p(k)$ can be written in the

form

$$\phi_p(k) = \delta_{k,p} + \frac{\mathrm{sgn}\,[F(k)]\,|F(k)|^{1/2}\,T(k,p)\,|F(p)|^{1/2}}{E_p - E_k + i\delta}\,, \tag{3.12}$$

where $T(k,p)$ is the on-shell T-matrix defined through

$$T(k,p)\,|F(p)|^{1/2} = -\sum_{k'} V_s(k-k')\,|F(k')|^{1/2}\,\phi_p(k')\,. \tag{3.13}$$

Substituting 3.13 into 3.12 the BSE for the on-shell T-matrix is obtained

$$T(k,p) = -V_s(k-p) - \sum_{k'} V_s(k-k')\frac{F(k')}{E_p - E_k + i\delta}T(k',p)\,. \tag{3.14}$$

Using the method developed by Noyes[66] the BSE can be transformed into a new nonsingular integral equation. The solution for T is written as $T(k,p) = T(p,p)f(k,p)$, where the function $f(k,p)$ satisfies

$$f(k,p) = \frac{V_s(k,p)}{V_s(p,p)} - \sum_{k'}\left[V_s(k,k') - \frac{V_s(k,p)V_s(p,k')}{V_s(p,p)}\right]\frac{F(k')}{E_p - E_{k'}}f(k',p) \tag{3.15}$$

and

$$T(p,p) = \frac{-V_s(p,p)}{1+\Lambda_1(p)} \tag{3.16}$$

with

$$\Lambda_1(p) = \sum_k V_s(p,k)f(k,p)\frac{F(k)}{E_p - E_k + i\delta}\,. \tag{3.17}$$

Note that the kernel of 3.15 is finite for $k' = p$ and $f(p,p) = 1$. The oscillator strength for transitions into scattering states is determined by

$$\sum_k |F(k)|^{1/2}\,\phi_p(k) = |F(k)|^{1/2}\left[1 - \frac{\Lambda_2(p)}{1+\Lambda_1(p)}\right]\,, \tag{3.18}$$

where

$$\Lambda_2(p) = \sum_k V_s(p,p)f(k,p)\frac{F(k)}{E_p - E_k + i\delta}\,. \tag{3.19}$$

The absorption, gain, and luminescence are given respectively as $D(\omega)$, $-D(\omega)$,

and

$$D(\omega)/\left[\exp\left[(\omega-\mu/T)\right]-1\right],$$

where $D(\omega)$ is the interband density of states. The interband density of states is obtained from the imaginary part of the retarded $e-h$ pair propagator

$$D(\omega) = -\mathrm{Im}\sum_{k,k'} G(k,k',\omega)\,. \tag{3.20}$$

Substituting Eqn. 3.18 in Eqn. 3.11, the interband density of states can be written as

$$D(\omega) = D_0(\omega)\rho(\omega) \tag{3.21}$$

where

$$D_0(\omega) = \pi\sum_p F(p)\delta(\omega - E(p)) \tag{3.22}$$

is the one-particle result and

$$\rho(\omega) = \left|1 - \frac{\Lambda_2(p)}{1+\Lambda_1(p)}\right|^2_{E(p)=\omega} \tag{3.23}$$

is the excitonic enhancement due to the multiple $e-h$ scattering.

3.2 Low Temperature Limit

In the limit $T \ll E_0$ the picture of an electron-hole pair embedded in the electron-hole plasma is completely misleading, as the screening of attractive Coulomb forces is governed mainly by bound states. These are much less efficient in their screening than free carriers due to the gap in their excitation spectrum. Thus, the bound state concentration needed to ionize an exciton is much larger than the corresponding free carrier concentration. Other complications due to the low temperature arise when electronic excitations undergo a Bose-Einstein condensation, which is expected in the framework of equilibrium thermodynamics.[65] These are classified with respect to the biexciton radius a_m:

in the very dilute limit $N^{-1} \gg a_m$, the ground state should consist of condensed biexcitons. Above the biexciton ionization threshold $N^{-1} \sim a_m$ ordinary exciton condensation should set in. For densities above the exciton ionization threshold $N^{-1} \sim a_0$ (exciton radius), the formation of a normal electron-hole plasma or of a dielectric electron-hole liquid consisting of electron-hole Cooper pairs is expected.

3.3 Discussion

In the quasi-one-dimensional systems, the Sommerfeld factor which describes the deviations of the continuum spectrum from the free carrier spectrum, is smaller than unity for all $\hbar\omega > E_g$, in striking contrast to the 3D and 2D cases. Due to this fact, the singularities of one dimensional density of states do not show up in the absorption spectrum. The absence of any structure at the band-gap is by no means a consequence of a finite broadening but is solely a Coulomb effect. Practically, the entire oscillator strength is accumulated in the exciton ground state.

In chapter 2, we have considered the many-body effects on the band-gap due to electrons and holes generated by intense photo-excitation. The results which are based on a well-established theory implies a band-gap renormalization of the order of tens of meV's. On experimental side, the measured band-gap renormalization were, however, always less than the predictions of theory. A number of recent experimental observations[24,48] reported that the photoluminescence emitted from an initially photo-excited semiconductor quantum wire plasma peaks essentially at a *constant* energy independent of the magnitude of the photo-excitation intensity. In view of theoretical predictions, this is surprising, because one expects a strongly density-dependent red-shift in the peak due to the exchange-correlation induced band-gap renormalization. This lack of any dependence of the photo-excitation peak on the photo-excitation has led to the suggestion that the observed quantum wire photoluminescence may be due entirely to an excitonic mechanism (as opposed to an electron-hole plasma recombination mechanism). Further, the effective excitonic energy does not depend on the

carrier density in quantum wires. This, however introduces a new puzzle because one expects the excitonic level to exhibit a blue-shift (i.e. an increase) as a function of carrier density as the Coulomb interaction weakens due to screening by the finite carrier density leading to a diminished excitonic binding energy. An explanation is based on a cancellation of the red-shift arising from the self-energy correction induced band-gap renormalization by the blue-shift arising from screening induced excitonic binding weakening. Das Sarma and Wang[64] studied this mechanism within a many-body theoretical formalism. In their work, the solution of the Bethe-Salpeter equation for the electron-hole pair propagator is presented in the presence of dynamically screened Coulomb interaction. Fig.3.2 shows their results. In the full dynamical result, the calculated absorption spectrum has negligible shift, consistent with experimental results. It is therefore important to emphasize the importance of dynamical correlations in comparison with the quasi-static approximation. The optical absorption spectrum calculated in the quasi-static approximation shows that, the excitonic peak has a slight red-shift combined with a rapid decrease at the oscillator strength with increasing density. In contrast to that, the dynamical formulation predicts no significant shift at the peak position. At the same time, the strength of the exciton peak remains almost a constant with increasing density, indicating the interesting prospect of excitonic lasing in quantum wires.

Finally, we would like to discuss the Mott transition in a quasi-one-dimensional system. We have seen that with increasing $e-h$ plasma density, the band-gap gets renormalized and shrinks, whereas the exciton binding energy level stays more or less constant (in the quasi-static formulation, the binding energy is also red-shifted, but this happens slower than the band-gap shift). The point, where the bound state energy merges with the band continuum yields the value of the so called Mott density. After this point, the exciton becomes unstable and the electron-hole pair dissociates. Therefore, the Mott transition may be thought effectively as an interaction-induced insulator to metal transition which occurs as the exciton gas becomes an electron-hole plasma at Mott density. The dynamical formulation predicts the transition at a lower density than that

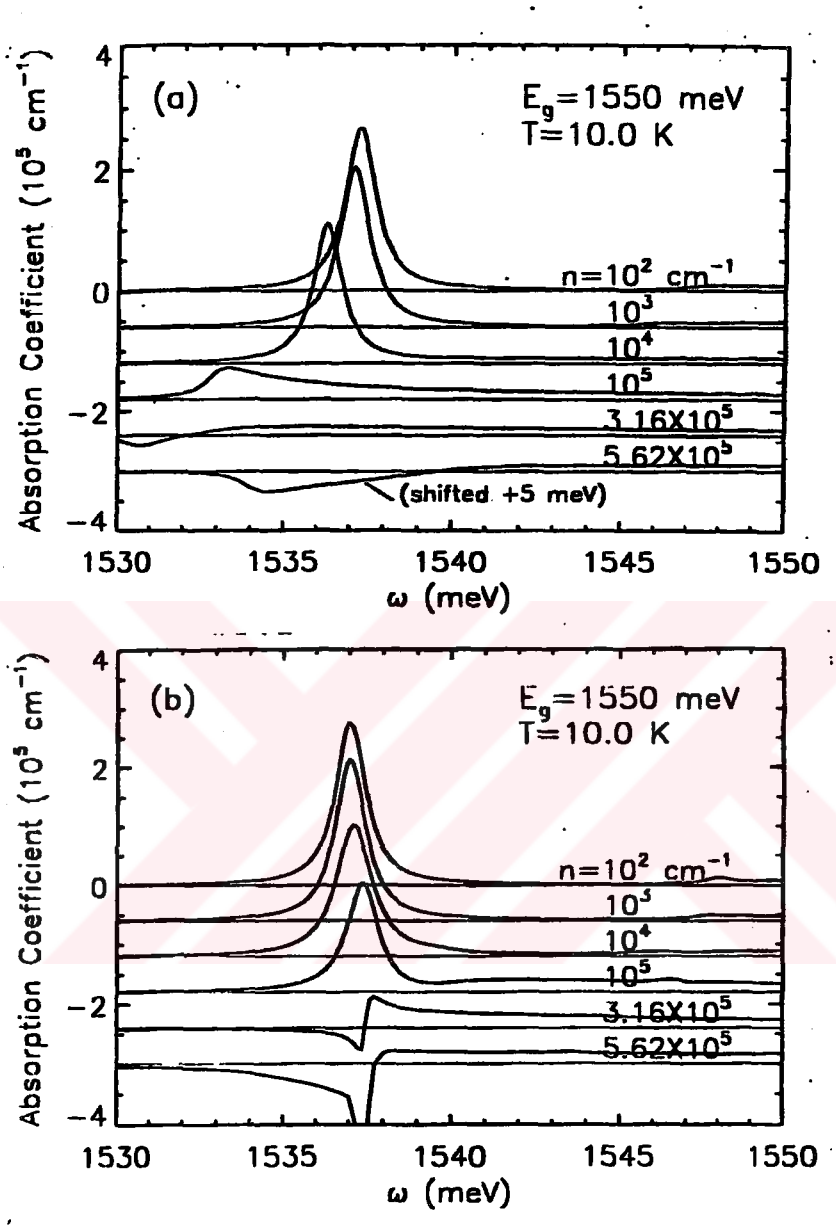

Figure 3.2: Calculated absorption spectra for a GaAs quantum wire structure for various photo-excitation densities by solving the full Bethe-Salpeter equation (a) quasi-static approximation, (b) dynamical approximation. (after Das Sarma *et. al.*[64])

of usually quoted in the literature for GaAs quantum wire systems.

Chapter 4

General conclusions

Under photo-excitation above the band-gap, both excitons and unbound electron-hole pairs are generated in a semiconductor quantum wire, which are interacting. How does this interaction affect the photoluminescence spectrum of the system? A single formalism which grasps this problem in all aspects is practically intractable. It is then necessary to deal with the problem piecewise, and resort to some approximations, which can be justified experimentally. In this thesis work, we have investigated the interaction effects within the framework of many-body theory. For a dense $e-h$ plasma system, the exchange-correlation effects can be treated by the perturbation theoretical approach.

First, we considered the exchange-correlation effects in $e-h$ plasma alone. Many-body theoretical formalism implies a renormalization of the band-gap, which is induced by self-energy correction due to exchange-correlation effects. The renormalization depends strongly on the density of $e-h$ plasma, and increases with increasing density up to $\sim$ 60 meV. We have considered the renormalization in a two-subband formulation. The most sophisticated approximation we have used in calculating screened Coulomb interaction is the full dynamic, temperature dependent random-phase approximation. The main achievements for this part are summarized as follows;

- The subband structure affects the renormalization. Even in the simple two-subband formulation, the very presence of the second subband affects the

renormalization process.

- The dynamical nature of screening produces significant changes compared to quasi-static screening.
- The subband renormalization is rather insensitive to changes in temperature.
- Coupling to bulk LO-phonons can be well accounted for by the ε_0-approximation

The next question was whether this renormalization should be observable in the photoluminescence spectrum of a quantum wire. This question should be considered with respect to the Mott transition point. For very high plasma densities ($n > 10^6$ cm^{-1}), when the excitons are completely ionized, the renormalization should reflect itself on the photoluminescence spectrum. For intermediate densities, however, there were comparable number of experimental studies with conflicting results on the presence of bandgap renormalization. In this case, precise assessment of the Mott transition point is essential. This is because, it was shown[60] that the Sommerfeld factor in the quantum wires is smaller than unity, hence when the excitons are present, they would dominate the low-energy part of the spectra.

If the photoluminescence peaks are due to excitonic recombination, it is necessary to explain: (1) how the excitons survive against the remarkably high $e-h$ plasma density; (2) why the exciton peak position remains constant throughout a wide density range. A sophisticated many-body theoretical formalism which takes *both* the band-gap renormalization and the exciton binding energy renormalization into account, might give the answers. One recipe for this formalism is based on the solution of the Bethe-Salpeter equation (Eqn.3.1) with a screened Coulomb interaction. Due to complicated nature of this equation, the screened interaction among the pairing electron and hole is usually approximated by the quasi-static approximation. We have formulated the equation for a quasi-one-dimensional system, but refrained from the numerical implementation,

mainly because, for 2D quantum wells[53] and recently for quantum wires[64] this formulation is shown to exhibit a red-shift (i.e. reduction) in the excitonic level, too. A necessary step is then to utilize the full dynamical approximation to see whether the reason of nearly constant nature of the excitonic binding energy is related to dynamical screening effects. This was beyond the scope of the work in this thesis. Very recently, such dynamical formalism is presented by Das Sarma and Wang.[64] It is shown that the renormalization of the band-gap is compensated by the counter-renormalization of the exciton binding energy leading essentially to a constant position for the excitonic peak in the photoluminescence spectrum. Within the dynamical formalism, the Mott transition occurs at considerably higher plasma density compared to the value predicted by the quasi-static approximation. Based on these results, we conclude that the dynamical nature of correlations are crucial for a correct description of nonlinear optical properties in a quantum wire.

Another formalism employed in studying renormalization effects in quantum wires is the density functional theory (DFT).[70] In particular, this method gives comparable bandgap renormalization to that derived in many-body theory. In comparison to many-body formalism, DFT can handle the geometrical factors (e.g. the quantum confined Stark effect) which are usually ignored in the many-body formalism. The drawback of DFT is that, it forsakes the phonon-carrier and the dynamics of screening.

Finally, we would like to point out possibilities for future progress. The many-body theoretical formalism is based on several approximations which restrict the application of the formalism in certain aspects. Hence, by using more sophisticated approximations, the formalism can be improved and extended to a wider range. For example, the GW-approximation we have used in calculating the bandgap renormalization can be improved for the lower density range by using vertex corrections. In calculating the LO-phonon coupling effects, only the bulk LO-phonons are considered in this work. The confined phonon effects for a quasi-one-dimensional electron hole system in the single subband model is considered elsewhere.[22] It might be interesting to consider the confined optical phonon effects

within this two subband formalism, when a particular phonon mode has energy equal to the energy difference of electronic subbands. By using the self-consistent electronic structure of a particular quantum wire, realistic subbands and effective Coulomb interaction elements can be obtained, which improve the quantitative results of the theoretical formalism.

Bibliography

[1] H. Sakaki, "Scattering suppression and high mobility effect of size-quantized electrons in ultrafine semiconductor wire structures", Jpn. Appl. Phys. **19**, L735-L738 (1980).

[2] P. M. Petroff, A. C. Gossard, R. A. Logan, and W. W. Wiegmann, "Toward quantum well wires - Fabrication and optical properties", Appl. Phys. Lett. **41** 635 (1982).

[3] T. Demel, D. Heitmann, P. Grambow, and K. Ploog, "Far-infrared response of one dimensional electronic systems in single layered and double layered quantum wires", Phys. Rev. B **38**, 2732 (1988).

[4] J. Christen, M Grundmann, E. Kapon, E. Colas, D. M. Hwang, and D. Bimberg, "Ultrafast carrier capture and long recombination lifetimes in GaAs quantum wires grown on nonplanar substrates", Applied Physics Letters **61**, 67 (1992).

[5] S. Tomonaga, "Remarks on Bloch's Method of Sound Waves applied to Many-Fermion Problems", Prog. Theor. Phys. **5**,349 (1950).

[6] J. M. Luttinger, 'An exactly solvable model of a many fermion system", Journ. of Math. Phys. **4**, 1154 (1963).

[7] B. Y.-K. Hu and S. Das Sarma, "Many-body properties of a quasi-one-dimensional semiconductor quantum wire", Phys. Rev. Lett. **68**, 1750 (1992); "Many-body exchange-correlation effects in the lowest subband of semiconductor quantum wires", Phys. Rev. B **48**, 5469 (1993).

[8] S. Benner and H. Haug, "Plasma density dependence of the optical spectra for quasi-one-dimensional quantum well wires, Europhys. Lett. **16**, 579 (1991).

[9] B. Tanatar, "Band gap renormalization in quasi-one-dimensional electron-hole systems", J. Phys. Condens. Matter **8**, 5997 (1996).

[10] K. H. Wang, M. Bayer, A. Forchel, P. Ils, S. Benner, H. Haug, Ph. Pagnod-Rossiaux, and L. Goldstein, "Subband renormalization in dense electron-hole plasmas in $In_{0.53}Ga_{0.47}As/InP$ quantum wires, Phys. Rev. B **53**, 10505.

[11] M. Grundman, J. Christen, M. Joschko, D. Bimberg, and E. Kapon, "Band gap renormalization in quantum wires", in D. J. Lockwood (ed.) *The Physics of Semiconductors*, World Scientific, Singapore, p. 1675 (1995).

[12] H. Haug and S. Schmitt-Rink, "Electron theory of the optical properties of laser-excited semiconductors", Prog. Quant. Elec. **9**, 3 (1984).

[13] H. Haug and S. Schmitt-Rink, "Basic mechanisms of the optical nonlinearities of semiconductors near the band edge", J. Opt. Soc. Am. B **2**, 1135 (1985).

[14] S. Schmitt-Rink, C. Ell, S. W. Koch, H. E. Schmidt, and H. Haug, "Subband level renormalization and absorbative optical bistability in semiconductor multiple quantum well structures", Solid State Comm. **52**, 123 (1984).

[15] G. Tränkle, C. Ell, A. Forchel, G. Griffiths, H. Haug, H. Krömer, E. Lach, F. Scholz, S. Subbanna, G. Weimann, "General relation between band gap renormalization and carrier density in two dimensional electron hole plasmas", Phys. Rev. B **36**, 6712 (1987); *ibid.* G. Tränkle, C. Ell, A. Forchel, H. Haug, H. Leier, G. Weimann, "Dimensionality dependence of the band gap renormalization in two-dimensional and 3-dimensional electron-hole plasmas in GaAs", Phys. Rev. Lett. **58**, 419 (1987).

[16] C. Weber, C. Klingshirn, D. S. Chemla, D.A.B. Miller, J. E. Cunningham, C. Ell, "Gain measurements and band gap renormalization in GaAs/$Al_xGa_{1-x}As$ multiple quantum well structures", Phys. Rev. B **38**, 2748 (1988).

[17] V. D. Kulakovskii, E. Lach, A. Forchel, D. Grutzmacher, "Band gap renormalization and band filling effects in a homogeneous electron-hole plasma in $In_{0.53}Ga_{0.47}As$/InP single quantum wells", Phys. Rev. B **40**, 8087 (1989).

[18] V. B. Campos, M. H. Degani, and O. Hipólito, "Exchange and correlation effects in a semiconductor quantum well wire", Superlatt. Microstruct. **17**, 85 (1995).

[19] K. S. Singwi, M. Tosi, R. H. Land, and A. Sjölander, "Electron correlations at metallic densities", Phys. Rev. B **176**, 589 (1968).

[20] Nguyen Trung Dan, F. Bechstedt, "Optical phonon effect in quasi one dimensional semiconductor quantum wires: Band-gap renormalization", Physica B **219**, 47 (1996).

[21] E. H. Hwang and S. Das Sarma, "Band-gap renormalization in photo-excited semiconductor quantum-wire structures in the *GW* approximation", Phys. Rev. B **58**, R1738 (1998).

[22] C. R. Bennett, K. Güven, B. Tanatar, "Confined optical phonon effects on the band-gap renormalisation in quantum wire structures", Physica B **263-264**, 546 (1999).

[23] D. B. Tran Thoai and H. T. Cao, "Band-gap renormalization of photoexcited quantum-well wires", Solid State Commun. **109**, 413 (1999).

[24] R. Ambigapathy, I. Bar-Joseph, D. Y. Oberli, S. Haacke, M. J. Brasil, F. Reinhardt, E. Kapon, and B. Deveaud, "Coulomb correlation and band gap

renormalization at high carrier densities in quantum wires", Phys. Rev. Lett. **78**, 3579 (1997).

[25] T. Ando, A. B. Fowler, and F. Stern, "Electronic properties of two-dimensional systems", Rev. Mod. Phys. **54**, 437 (1982).

[26] L. Hedin and S. Lundqvist in *Solid State Physics* ed. H. Ehrenreich F. Seitz, and D. Turnbull, (Academic. NY 1969), vol. 23.

[27] R. Rinaldi, R. Cingolani, L. DeCaro, M. Lomascolo, M. DiDio, L. Tapfer, U. Marti, and F. K. Reihart, "Optical spectroscopy if InGaAs/GaAs V-shaped quantum wires", J. Opt. Soc. Am. B **13**, 1031 (1996).

[28] S. A. Laux and F. Stern, Appl. Phys. Lett. **49**, 91 (1986).

[29] C. R. Proetto, "Self consistent electronic structure of a cylindrical quantum wire", Phys. Rev. B **45**, 11911 (1992).

[30] A. Gold and A Ghazali, "Analytical results for semiconductor quantum-well wire: plasmons, shallow impurity states, and mobility", Phys. Rev. B **41**, 7626 (1990).

[31] G. D. Mahan, *Many-Particle Physics*, 2nd ed. (Plenum N.Y. 1990), chapters 4,5.

[32] E. H. Hwang, and S. Das Sarma, "Collective excitations of a two-component one-dimensional quantum plasma confined in semiconductor quantum wires", Phys. Rev. B **50**, 17267 (1994).

[33] L. Hedin, "New method for calculating the one-particle Green's function with application to the electron-gas problem", Phys. Rev. **139**, A796 (1965).

[34] G. D. Mahan and B. E. Sernelius, "Electron-electron interactions and the bandwidth of metals", Phys. Rev. Lett. **62**, 2718 (1988).

[35] H. O. Frota, G. D. Mahan, "Band tails and bandwidth in simple metals", Phys. Rev. B **45**, 6243 (1992).

[36] J. K. Lindhard, Dan. Vidensk. Selsk. Mat. Fys. Medd, **28**, (8) 1954.

[37] P. Maldague, "Many-body corrections to the polarizability of the two dimensional electron gas", Surface Science **73**, 296 (1978).

[38] F. B. Hildebrand, *Advanced Calculus for Applications*, Prentice-Hall (1976), p. 592 .

[39] I. K. Marmorkos and S. Das Sarma, "Many-body vertex corrections on quasiparticle properties of two-dimensional electron systems", Phys. Rev. B **44**, 3451 (1991).

[40] G. D. Mahan, "Excitons in degenerate semiconductors", Phys. Rev. **153**, 882 (1967).

[41] Y. Arakawa and H. Sakaki, "Multidimensional quantum well laser and temperature dependence of its threshold current", Appl. Phys. Lett. **40**, 939 (1982).

[42] E. Kapon, "Quantum wire lasers", Proc. IEEE **80**, 398 (1992).

[43] S. Nojima, "Dimensionality of exciton-state renormalization in highly excited semiconductors", Phys. Rev. B **51**, 11124 (1995).

[44] S. Schmitt-Rink, D. S. Chemla, and D. A. B. Miller, "Linear and nonlinear optical properties of semiconductor quantum wells", Adv. Phys. **38**, 89 (1989).

[45] R. Cingolani, H. Lage, L. Tapfer, H. Kalt, D. Heitmann, and K. Ploog, "Quantum confined one-dimensional electron-hole plasma in semiconductor quantum wires", Phys. Rev. Lett. **67**, 891 (1991).

[46] R. Cingolani, R. Rinaldi, A. Ferrara, G. C. LaRocca, H. Lage, D. Heitmann, K. Ploog, and H. Kalt, "Band-gap renormalization in quantum wires", Phys. Rev. B **48**, 14331 (1993).

[47] I.S.Gradstehyn, I.M.Ryzhik, *Table of Integrals, Series, and Products*, ed. A. Jeffrey, Fifth Edition, Academic Press, p. 44 (1994).

[48] W. Wegscheider, L. N. Pfeiffer, M. M. Dignam, A. Pinczuk, K. W. West, S. L. McCall, and R. Hull, "Lasing from excitons in quantum wires", Phys. Rev. Lett. **71**, 4071 (1993).

[49] R. Rinaldi, G. Coli, A. Passaseo, R. Cingolani, "Band-gap renormalization in modulation doped $In_{1-x}Ga_xAs/GaAs$ V-shaped quantum wires", Phys. Rev. B **59**, 2230 (1999).

[50] S. Das Sarma, R. Jalabert, and S. R. E. Yang, "Band-gap renormalization in quasi-two-dimensional systems induced by many-body electron-electron and electron-phonon interactions", Physical Review B **39**, 5516 (1989); *ibid.* "Band-gap renormalization in quantum-wells", **41**, 8288 (1990)

[51] J. J. Quinn and R. A. Ferrell, "Electron self-energy approach to correlation in a degenerate electron gas", Phys. Rev. **112**, 812 (1958).

[52] K. Güven and B. Tanatar, "Simplified calculations of band-gap renormalization in quantum-wells, Superlatt. Microstruct. **20**, 81 (1996); and references therein.

[53] S. Schmitt-Rink, C. Ell, and H. Haug, "Many-body effects in the absorption, gain, and luminescence spectra of semiconductor quantum-well structures", Phys. Rev. B **33**, 1183 (1986).

[54] S. Glutsch, F. Bechstedt, W. Wegscheider, and G. Schedelbeck, "Excitons in T-shaped quantum wires", Phys. Rev. B **56**, 4108 (1997).

[55] D. Brinkmann and G. Fishman, "Exciton Rydberd in T-shaped quantum wires", Phys. Rev. B **56**, 15211 (1997).

[56] S. N. Walck, T. L. Reinecke, P. A. Knipp, "Exciton binding energy in T-shaped quantum wires", Phys. Rev. B **56**, 9235 (1997).

[57] F. Rossi and E. Molinari, "Linear and nonlinear optical properties of realistic quantum-wire structures: the dominant role of Coulomb correlation", Phys. Rev. Lett. **53**, 16462 (1996); F. Rossi *et al. ibid.* **56**, 3527 (1997).

[58] F. Tassone and C. Piermarocchi, "Electron-hole correlation effects in the emission of light from quantum wires", Phys. Rev. Lett. **82**, 843 (1999).

[59] S. Benner and H. Haug, "Influence of electric and magnetic fields on the excitonic absorption spectra of quantum-well wires", Phys. Rev. B **47**, 15570 (1993).

[60] T. Ogawa and T. Takagahara, "Optical absorption and Sommerfeld factors of one-dimensional semiconductors: an exact treatment of excitonic effects", Phys. Rev. B **44**, 8138 (1991).

[61] C. Piermarocchi, V. Savona, A. Quattropani, P. E. Selbmann, P. Schwendimann, and F. Tassone, "Photoluminescence spectra in semiconductor confined systems: Effects of Coulomb correlation", Phys. Stat. Sol. (b) **206**, 455 (1998).

[62] R. Schepe, T. Schmielau, D. Tamme,and K. Henneberger, "Damping and T-matrix in dense e-h plasmas", Phys. Stat. Sol. (b) **206**, 273 (1998).

[63] D. O. Gericke, S. Kosse, M. Schlanges, and M. Bonitz, "Strong correlation (T-matrix) effects in electron-hole plasma in semiconductors", Phys. Stat. Sol. (b) **206**, 257 (1998).

[64] S. Das Sarma and D. W. Wang, "Many-body renormalization of semiconductor quantum wire excitons: absorption, gain, binding, unbinding, and Mott transition", cond-matt/9905038, 1999.

[65] E. Hanamura and H. Haug, Phys. Rep. **33C**, 209 (1977).

[66] H. P. Noyes, "New nonsingular integral equation for two-particle scattering", Phys. Rev. Lett. **15**, 538 (1965).

[67] H. Lage, D. Heitmann, R. Cingolani, P. Grambow, and K. Ploog, "Center-of-mass quantization of excitons in quantum-well wires", Phys. Rev. B **44**, 6550 (1991).

[68] K. Brunner, G. Abstreiter, M. Walther, G. Böhm, and G. Tränkle, " ", Surf. Sci. **267**, 218 (1992).

[69] R. Rinaldi, R. Cingolani, M. Lepore, M. Ferrara, I. M. Catalano, F. Rossi, L. Rota, E. Molinari, P. Lugli, U. Marti, D. Martin, F. Morier-Gemoud, P. Ruterana, and F. K. Reinhart, "Exciton binding energy in GaAs V-shaped quantum wires", Phys. Rev. Lett. **73** 2899 (1994).

[70] M. Stopa, "Bandgap renormalization and excitonic binding in T-shaped quantum wires", cond-mat/9908349, 1999.